Microtubule-targeting drugs rescue axonal swellings in cortical neurons from spastin knockout mice

Coralie Fassier, Anne Couturier-Tarrade, Leticia Peris, Sabrina Courageot, Philippe Mailly, Cécile Dalard, Stéphanie Delga, Natacha Roblot, Julien Lefèvre, Didier Job, et al.

Microtubule-targeting drugs rescue axonal swellings in cortical neurons from spastin knock-out mice

Coralie Fassier[1,4,*], Anne Tarrade[1,2], Leticia Peris[3], Sabrina Courageot[1], Philippe Mailly[4], Cécile Dalard[1], Stéphanie Delga[2], Natacha Roblot[1], Julien Lefevre[2], Didier Job[3], Jamilé Hazan[4], Patrick A. Curmi[2,*] and Judith Melki[1,*].

1 Inserm U798, Laboratoire de Neurogénétique moléculaire, Université d'Evry-Val d'Essonne et Paris XI, Evry, F-91057, France.

2 Inserm U829, Laboratoire Structure-Activité des Biomolécules Normales et Pathologiques, Université d'Evry-Val d'Essonne, Evry, F-91025 France.

3 Inserm U 836, Institut des Neurosciences de Grenoble, Université Joseph Fourier, Grenoble, F-38042, France

4 UMR CNRS 7224 / Inserm U952 / Université P. & M. Curie, Paris, F-75005, France.

Present address for J.M.: Inserm Unit 788 and University of Paris 11, Bicêtre Hospital, Gregory Pincus Building, 80 rue du Général Leclerc, Le Kremlin-Bicêtre 94276, France.

Present address for A.T.: INRA, UMR 1198 Biologie du Développement et Reproduction, F-78352 Jouy-en-Josas, France.

* To whom correspondence should be addressed:

Judith Melki: Tel: +331 4959 5370; Fax: +331 4959 1959; Email: judith.melki@inserm.fr

Patrick A Curmi: Tel: +331 6947 0187; Fax: +331 6947 0219; Email: pcurmi@univ-evry.fr

Coralie Fassier: Tel: +331 4427 3491; Fax: +331 4427 2508; Email: cfassier@snv.jussieu.fr

DMM Advance Online Articles. Published 5 July 2012 as doi: 10.1242/dmm.008946
Access the most recent version at http://dmm.biologists.org/lookup/doi/10.1242/dmm.008946

Abbreviations: HSP, hereditary spastic paraplegia; AAA, ATPase associated with diverse cellular activities; GFP, green fluorescent protein; CTb, Cholera toxin subunit B; NSC-34, neuroblastoma x spinal cord 34; DIV, day *in vitro*; RNAi, RNA interference.

Abstract

Mutations in *SPG4,* encoding the microtubule-severing protein spastin, are responsible for the most frequent form of hereditary spastic paraplegia (HSP), a heterogeneous group of genetic diseases characterized by degeneration of the corticospinal tracts. We previously reported that mice harboring a deletion in *Spg4*, generating a premature stop codon, develop progressive axonal degeneration characterized by focal axonal swellings associated with impaired axonal transport. To further characterize the molecular and cellular mechanisms underlying this mutant phenotype, we have here assessed microtubule dynamics and axonal transport in primary cultures of cortical neurons from spastin mutant mice. We show an early and marked impairment of microtubule dynamics all along the axons of spastin-deficient cortical neurons, which is likely to be responsible for the occurrence of axonal swellings and cargo stalling. Our analysis also reveals that a modulation of microtubule dynamics by microtubule-targeting drugs rescues the mutant phenotype of cortical neurons. Altogether, these results contribute to a better understanding of the pathogenesis of *SPG4*-linked HSP and ascertain the influence of microtubule-targeted drugs on the early axonal phenotype in a mouse model of the disease.

Key words: hereditary spastic paraplegia, spastin, microtubule-severing enzyme, axonal transport, knock-out mouse model, microtubule-targeting drugs

Running title: Microtubule dynamics and spastin mutant mice

Translational Impact Box

(1). *Clinical issue*: Hereditary spastic paraplegia (HSP) is a heterogeneous group of neurodegenerative disorders mainly characterized by progressive and bilateral spasticity of the lower limbs due to the retrograde degeneration of the corticospinal tracts. Among the numerous HSP proteins, spastin, encoded by the most common gene for the disease, is altered in 40% of all autosomal dominant HSP families. We have here further characterized the pathogenic process occurring in a mouse model of the disease that develops a progressive axonal degeneration of cortical neurons.

(2). *Results*: Using primary cultures of cortical neurons from our spastin mutant mice, we explored the molecular and cellular mechanisms underlying the axon swelling phenotype, which precedes the degeneration of cortical axons. Our analysis reveals a marked and specific impairment of microtubule dynamics in spastin-depleted cortical axons, which is associated with a major disorganization of the microtubule network within the swellings that significantly alters axonal transport. Furthermore, we show that very low concentrations of microtubule-targeting drugs substantially rescue the axon phenotype associated with a loss of spastin function in mammalian cortical neurons, which thereby indicates that alterations in microtubule dynamics primarily give rise to the mouse mutant phenotype.

(3). *Implications and future directions*: Although the molecular bases underlying the rescue of mouse mutant neurons by these drugs need to be further dissected, our results provide new insights into potential suppressors of the early axonal phenotype in a mammalian model of HSP, which may orientate future development of therapeutic strategies.

Introduction

Hereditary spastic paraplegia (HSP) is a heterogeneous group of inherited neurological disorders mainly characterized by a bilateral and slowly progressive spasticity of the lower limbs caused by the degeneration of the corticospinal tracts (Reid, 2003; Fink, 2006). HSP shows a considerable genetic heterogeneity with 45 loci mapped so far (Salinas *et al*., 2008). Mutations in the *SPG4* gene encoding spastin, a member of the AAA ("ATPase Associated with diverse cellular Activities") superfamily, are responsible for the most frequent form of autosomal dominant HSP (Hazan *et al*., 1999). More than 200 mutations have been described within *SPG4* coding sequence including nonsense, frameshift, splice site, missense mutations as well as large-scale deletions (Hazan *et al*., 1999; Fonknechten *et al*., 2000; Depienne *et al*., 2007). Although some missense mutations clearly show a dominant-negative effect (Errico *et al*., 2002; Du *et al*., 2010; Solowska *et al.,* 2010), the vast majority of *SPG4* mutations, which affect the ATPase domain, were suggested to cause this form of HSP by haploinsufficiency (Fonknechten *et al.*, 2000; Charvin *et al.*, 2003; Roll-Mecak and Vale, 2008; Riano *et al*., 2009).

The *SPG4* gene directs the synthesis of four spastin isoforms through the use of alternative translation initiation sites, which generate a full-length protein of 68 kDa and a shorter isoform of 60 kDa, in addition to the alternative splicing of exon 4, which leads to two additional isoforms of 64 and 56 kDa respectively (Claudiani *et al*., 2005). Like p60-katanin, spastin is involved in microtubule severing (Errico *et al*., 2002; Evans *et al.,* 2005; Salinas *et al.*, 2005; Roll-Mecak and Vale, 2005), a process by which long microtubules are cut into shorter and highly motile fragments (Baas *et al*., 2005). Spastin forms a ring-shape hexamer containing a prominent central pore into which the C-terminal tail of tubulin is attached and pulled. It has been proposed that the mechanical forces exerted by spastin on the C-terminal tail of tubulin destabilize tubulin-tubulin interactions in the microtubule lattice (White *et al.*,

2007; Roll-Mecak and Vale, 2008). In the cytoplasm, spastin localizes to vesicular structures, tubular endoplasmic reticulum (ER) and predominantly to cellular regions characterized by extensive remodeling of the cytoskeleton such as the centrosomes, the spindle poles and the mitotic cell midbody, in addition to neuron growth cones and axon branch points (Errico *et al*., 2004; Yu *et al*., 2008; Connell *et al*., 2009, Park *et al.*, 2010). In neurons, spastin and katanin microtubule-severing activities provide an important source of non-centrosomal microtubules and were shown to be essential for axon outgrowth and branching *in vitro* (Karabay *et al*., 2004; Riano *et al*., 2009; Yu *et al*., 2008). Functional studies in zebrafish and *Drosophila* revealed that spastin regulation of microtubule dynamics is crucial for motor neuron development and function (Wood *et al*., 2006; Trotta *et al*., 2004; Sherwood *et al*., 2004; Orso *et al*., 2005). We and others have reported that mice harboring an *SPG4*-truncated mutation develop a progressive axonal degeneration characterized by axonal swellings associated with impaired axonal transport (Tarrade *et al.*, 2006; Kasher *et al.*, 2009). Using primary cultures of cortical neurons from spastin mutant mice, we have shown that these axonal swellings occur in a specialized region of the axon characterized by an abrupt transition between stable and dynamic microtubules, which suggested that alterations in microtubule dynamics primarily give rise to this mutant phenotype (Tarrade *et al.*, 2006). However no experimental evidence supporting this hypothesis has been brought forward so far, whereas other pathogenic mechanisms, including defective membrane trafficking or impaired ER morphogenesis, were also suggested to cause axonopathy in cell and animal models of *SPG4*-linked HSP (for reviews, see Blackstone *et al*., 2011 and Lumb JH *et al*., 2012).

In the present study, we further analyzed primary cultures of cortical neurons from spastin mutant mice to determine the molecular and cellular mechanisms underlying the axon swelling phenotype. Our analysis reveals an early, marked and specific impairment of

microtubule dynamics in spastin-depleted cortical axons, which is associated with a major disorganization of the microtubule network within the swellings that alters retrograde axonal transport by increasing the frequency of cargo stalling. Furthermore, we show that nanomolar concentrations of microtubule-targeting drugs substantially rescue the axon phenotype associated with a loss of spastin function in mammalian cortical neurons.

Results

Loss of spastin function is the pathogenic model underlying the axonopathy of $Sp^{\Delta/\Delta}$ mouse mutant

We previously generated mice that carry a heterozygous ($Sp^{\Delta/+}$) or homozygous ($Sp^{\Delta/\Delta}$) deletion of *Spg4* exons 5 to 7, which leads to a premature stop codon and mimicks 15% of the truncated mutations found in HSP patients (Tarrade *et al*., 2006). We initially reported that our heterozygous mice $Sp^{\Delta/+}$ show a 50% decrease in wild-type spastin compared to controls and develop a milder phenotype than their homozygous siblings $Sp^{\Delta/\Delta}$, which suggests a causative mechanism of haploinsufficiency (Tarrade *et al*., 2006). However, since haploinsufficiency was recently questioned for *SPG4*-linked HSP (Solowska *et al*., 2008), we tried to further characterize the molecular mechanism associated with the *Spg4* frameshift mutation of our mouse mutant by exploring whether $Sp^{\Delta/\Delta}$ mice express a truncated spastin lacking the AAA domain. We therefore carried out an immunoblot analysis of brain lysates from 4 month-old $Sp^{+/+}$, $Sp^{\Delta/+}$and $Sp^{\Delta/\Delta}$ mice using the S51 antibody, directed against the N-terminal region of spastin (from amino acids 87 to 354; Errico *et al*., 2004), which could thereby bind to the truncated protein. We also performed a control western blot with protein extracts from Cos-7 cells transfected with GFP-fused full-length or AAA domain-depleted spastin (GFP- Sp^{+} and GFP- Sp^{Δ}) (Fig. 1A). As expected, our analysis confirms that the S51 antibody recognizes the truncated spastin in transfected cells (GFP-Sp^{Δ}, Fig. 1A). However, $Sp^{\Delta/+}$ and $Sp^{\Delta/\Delta}$ mice do not show detectable levels of truncated spastin *in vivo*, while they exhibit a reduction (~40%) or a lack of wild-type spastin respectively (Fig. 1B and C). Furthermore, identical results were obtained with larger amounts of protein extracts (100 μg; data not shown), which thereby suggests that loss of spastin function might be responsible for the $Sp^{\Delta/\Delta}$ mutant phenotype.

Spastin mutation triggers axonal swellings in mouse cortical but not hippocampal neurons

Primary cultures of $Sp^{\Delta/\Delta}$ cortical neurons revealed the presence of swellings in the distal part of the axons at the proximity of the growth cone (Tarrade *et al*., 2006). To determine whether this phenotype is restricted to cortical neurons or could be observed in other neuronal populations, we analyzed primary cultures of hippocampal neurons, in which spastin is normally highly expressed (Ma *et al*., 2006), from $Sp^{+/+}$and $Sp^{\Delta/\Delta}$ mouse embryos. Hippocampal and cortical neurons were cultured in the same experimental conditions and processed at six days *in vitro* (DIV6) for acetylated α-tubulin immunolabeling. We first checked whether neurite outgrowth and branching were affected in $Sp^{\Delta/\Delta}$ hippocampal neurons, which is not the case since they behave similarly to $Sp^{+/+}$control neurons in that respect (Fig. 2A-B and data not shown). However, unlike $Sp^{\Delta/\Delta}$ cortical neurons, hippocampal neurons from $Sp^{\Delta/\Delta}$ mutant mice (n=4) do not show any axonal swellings in two independent experiments (Fig. 2B, G and H). To assess whether this observation was only due to a delayed occurrence of axonal swellings in these neurons, we analyzed the same experiments at DIV12 and confirmed the absence of swelling in cultured $Sp^{\Delta/\Delta}$ hippocampal neurons (data not shown). These data thus suggest that a lack of spastin specifically affects cortical axon integrity *in vitro*. We then tested whether the sensitivity of cortical neurons to *spg4* mutation could be explained by a cell-type specific expression of different spastin isoforms. To address this issue, we performed western blot analyses on 20 µg of total protein extracts from DIV6 cortical and hippocampal neurons using the S51 antibody (Errico *et al.*, 2004) that recognizes four spastin isoforms including the long (translated from the first ATG) and short (translated from the second ATG) isoforms with or without exon 4. A similar expression pattern was observed between these two neuronal cell types, with a predominant expression of the short exon 4-containing isoform and a seeming absence of the full-length isoforms (Fig. 2I). Therefore, the cell specificity of axonal swelling cannot be assigned to a differential

expression of spastin isoform(s). However, our findings show a selective sensitivity of mouse cortical neurons in response to the lack of spastin, which is consistent with the restricted phenotype observed in HSP patients.

Axonal transport is delayed in the distal region of $Sp^{\Delta/\Delta}$ cortical axons

We previously reported that mitochondria and peroxysomes were abnormally accumulated in the proximal part of neurite swellings, which suggested a focal impairment of retrograde axonal transport in $Sp^{\Delta/\Delta}$ cortical neurons (Tarrade *et al*., 2006). We have here further explored the subcellular distribution of various organelles, such as endosomes, lysosomes and synaptic vesicles and have showed that they are all accumulated within axonal swellings (Fig. S1A-C''), which indicates that the axonal transport defect of $Sp^{\Delta/\Delta}$ cortical neurons is generalized to several, if not all types of organelles. We next assessed retrograde axonal transport efficiency in primary cultures of $Sp^{\Delta/\Delta}$ cortical neurons using the Cholera Toxin b subunit (CTb). CTb is internalized at the growth cone and retrogradely transported to the soma where it accumulates in the endoplasmic reticulum and Golgi apparatus (Lencer *et al.*, 1999). Control $Sp^{+/+}$ and mutant $Sp^{\Delta/\Delta}$ cortical neurons were incubated with Alexa Fluor 488-conjugated CTb at DIV6 for 15 minutes and washed in CTb-free medium for 30 minutes or 3 hours. After fixation, we evaluated the percentage of CTb-treated neurons showing an accumulation of the fluorescent toxin in their soma. Surprisingly, no significant difference has been detected between the number of CTb positive $Sp^{+/+}$and $Sp^{\Delta/\Delta}$ neuron soma after 30 minutes or 3 hours of CTb washout (data not shown), suggesting that spastin depletion does not abolish retrograde axonal transport in cortical neurons. However, we observed an accumulation of CTb-positive vesicles in the proximal part of axonal swellings (Fig. S1D-D'') as previously reported for other organelles, which confirms that retrograde axonal transport is locally perturbed in $Sp^{\Delta/\Delta}$ cortical neurons.

To further characterize the deleterious effect of spastin depletion on axonal transport, we assessed mutant vesicular transport using phase-contrast video microscopy in DIV6 $Sp^{\Delta/\Delta}$ cortical neurons, with special emphasis on axonal swellings (Movie 1). We have shown that the vesicles located within axonal swellings displayed apparent Brownian motion, whereas vesicles in non-swollen axons exhibited rapid linear movements towards the cell soma. This Brownian motion, that is reminiscent of the microtubule-unloaded cargo movement, was non-linear and led to non-productive translocation of the vesicles, resulting in their progressive accumulation in the proximal part of the swellings (Movie 1). Moreover, we confirmed that retrograde axonal transport is not totally blocked in this specific region of the axon, since we clearly observed vesicles leaving the swelling and being retrogradely transported towards the soma in a rapid and linear way, which resembles the movement of microtubule-based transport. Our results thus demonstrate that spastin depletion does not abolish retrograde axonal transport but increases cargo stalling in axon swellings, possibly by locally disturbing cargo loading on microtubules.

Major disorganization of the microtubule network within axonal swellings of spastin-deficient cortical neurons

In $Sp^{\Delta/\Delta}$ cortical neurons, retrograde axonal transport is mainly impaired within and around the swellings. Since axonal swellings occur in a specific region of mutant axons, characterized by an abrupt transition between stable and dynamic microtubules (Tarrade *et al*., 2006), we examined whether this defect in axonal transport results from local perturbations of the microtubule network. To address this issue, we performed an ultrastructural study of axonal swellings with a special focus on microtubule architecture. Ultra-thin sections of DIV6 primary cultures of $Sp^{+/+}$ and $Sp^{\Delta/\Delta}$ cortical neurons were processed for electron microscopy. This analysis revealed a major disorganization of the

microtubule network within $Sp^{\Delta/\Delta}$ cortical axonal swellings, which displayed unbundled, misoriented and curly microtubules (Fig. 3A-F; arrows) compared to $Sp^{+/+}$ control axons where microtubules were organized in parallel arrays (Fig. 3G-H; arrows). Interestingly, we observed that some organelles are locally accumulated within the swellings but never entirely fill them, suggesting that swellings may primarily result from alterations of the microtubule network and not from an excessive accumulation of organelles (Fig. 3B and D). Our data thus indicate that spastin depletion affects microtubule organization in the distal part of cortical axons, which would lead to axonal transport defects within axon swellings.

Early and marked impairment of microtubule disassembly in spastin-deficient cortical neurons

We previously reported that a marker of stable microtubules (detyrosinated-tubulin) was accumulated within axonal swellings, which suggested an excessive stabilization of the microtubules in this specific region (Tarrade *et al*., 2006). To confirm this aberrant stabilization, we have first established that the microtubule-stabilizing protein Tau and delta 2-tubulin, a marker of very long-lived microtubules (Paturle-Lafanechère L *et al*., 1994) are similarly accumulated in the axonal swellings of $Sp^{\Delta/\Delta}$ cortical neurons (Fig. S2). To further demonstrate that spastin depletion leads to abnormal stabilization of the microtubule network, we compared the resistance of microtubules to the depolymerizing drug nocodazole in $Sp^{\Delta/\Delta}$ and $Sp^{+/+}$ cultured cortical neurons at DIV 4 (i.e. before the occurrence of neurite swellings). When DIV4 $Sp^{+/+}$or $Sp^{\Delta/\Delta}$ neurons were exposed to 30 μM nocodazole for 40 minutes, only residual tubulin staining was detectable in $Sp^{+/+}$ cortical axons whereas a persistent and strong signal could be observed in $Sp^{\Delta/\Delta}$ axons (Fig. 4A-H). To compare microtubule stability between the swellings and other regions of $Sp^{\Delta/\Delta}$ cortical axons, we performed another set of experiments in which DIV6 neurons were exposed to higher doses of nocodazole (40 μM) for

longer periods of time (30, 60 or 90 min; Fig. 4I-L and data not shown). We have preliminarily assessed that this longer treatment does not affect the survival of cortical neurons (data not shown). Interestingly, after a 90-minute exposure, the labeling of microtubules was barely detectable along the axon shaft whereas a strong signal persisted in $Sp^{\Delta/\Delta}$ axonal swelling (Fig. 4I-L). Altogether, our data show a marked and early impairment of microtubule disassembly all along the axon shaft of $Sp^{\Delta/\Delta}$ cortical neurons with an enhanced effect of microtubule stabilization within axonal swellings.

Spastin depletion decreases the number of microtubule plus ends in cortical axons

To assess whether the lack of microtubule severing reduces the number of dynamic plus ends within mutant cortical axons, we analyzed microtubule dynamics in $Sp^{+/+}$ and $Sp^{\Delta/\Delta}$ axons using the EB3-GFP fusion protein, which allowed us to visualize the plus ends of polymerizing microtubules (Stepanova T *et al*., 2003). EB3 belongs to the microtubule plus-end tracking protein family (+TIPs), which binds to rapidly growing microtubule plus ends and gradually dissociates from microtubules when they convert from polymerizing to a depolymerizing state. We electroporated $Sp^{+/+}$ and $Sp^{\Delta/\Delta}$ cortical neurons with an EB3-GFP construct and monitored the behavior of this fusion protein that appears as moving comets within axons (Stepanova T *et al*., 2003) by time-lapse videomicroscopy at DIV6 (Fig.5 and Movies 2-5). A total of 20 $Sp^{+/+}$ and 29 $Sp^{\Delta/\Delta}$ transfected axons were imaged and analyzed. Kymograph analysis of time-lapse recording revealed that the average number of EB3-GFP comets is significantly reduced in $Sp^{\Delta/\Delta}$ axons (61.47±4.16) compared to $Sp^{+/+}$ axons (95.26±9.35; $p<0.001$; Fig.5A-C). Furthermore, the vast majority of EB3-GFP comets were moving in the anterograde direction in both $Sp^{+/+}$ (98.97%) and $Sp^{\Delta/\Delta}$ axons (96.24%), while the number of retrogradely moving comets per 100 μm of axonal length was not significantly different between $Sp^{+/+}$ (1.31±0.80) and $Sp^{\Delta/\Delta}$ axons (1.77±0.88; p=0,071; data not shown).

Surprisingly, the mean velocity of EB3-GFP comets was not significantly decreased in $Sp^{\Delta/\Delta}$ axons (0.069±0.004) compared to $Sp^{+/+}$control axons (0.078 ±0.007 μm/sec; p=0.236; Fig.5D and Movies 2-5), which suggests that spastin depletion does not affect microtubule polymerization rate. We also investigated the behavior of EB3-GFP comets within $Sp^{\Delta/\Delta}$ axonal swellings, although the low frequency of swellings (~ 5 axon swellings per 100 nuclei) associated with the small percentage of transfected neurons expressing the appropriate level of the fusion protein prevented a statistical analysis of EB3-GFP comet dynamics in the swellings compared to control axons. However, kymograph analysis of 10-minutes time-lapse recording in two $Sp^{\Delta/\Delta}$ axonal swellings revealed that only very few EB3-GFP comets are moving within the swellings as shown for non-swollen $Sp^{\Delta/\Delta}$ axons and that the vast majority of these moving comets are found in the distal end of the swellings (Fig.5E and boxed regions of Movies 2, 4, 5).

Altogether, these results demonstrate that the loss of spastin microtubule-severing activity significantly impairs the number of dynamic microtubule plus ends within cortical axon shafts, without affecting the polymerization rate of the remaining plus ends.

Substoichiometric concentrations of microtubule-targeting drugs alleviate the pathological phenotype of spastin-deficient cortical neurons

Finally, we checked whether a modulation of microtubule dynamics could modify the pathological phenotype of $Sp^{\Delta/\Delta}$ cortical neurons. To preserve the overall architecture of neuron microtubule network, we used tubulin/microtubule-targeting drugs at nanomolar concentrations, which are known to only modify microtubule dynamic instability (Jordan and Wilson, 1990; Jordan *et al.*, 1991; Toso *et al.*, 1993; Jordan *et al.*, 1993; Tanaka *et al.*, 1995; Vasquez *et al.*, 1997, Witte *et al.,* 2008). $Sp^{\Delta/\Delta}$ neurons were treated before (DIV2) or as soon as the first swellings start to appear (DIV5; Tarrade *et al.*, 2006), with either 50 (DIV2) to 100

nM (DIV5) nocodazole, 10 nM vinblastine (DIV5), 10 nM taxol (DIV5) or DMSO (control vehicle), fixed at DIV6 and immunolabeled with an acetylated α-tubulin antibody. These nanomolar doses of microtubule-targeting drugs do not affect the viability of cultured $Sp^{A/A}$ cortical neurons at both DIV2 and DIV5, as determined by the mean percentage of apoptotic neurons with or without treatment in three independent experiments (n>1000 neurons in each condition, data not shown). Moreover, the number of neurite swellings per 100 nuclei was assessed in more than 1000 neurons per embryo (n=4) and for each experimental condition. Interestingly, we observed a significant and reproducible effect of the three microtubule-targeting agents on the number of axon swellings in $Sp^{A/A}$ cortical neurons. Treatment of mutant neurons at DIV5 with 100 nM nocodazole successfully rescues the pathological phenotype of these neurons, reducing the number of neurite swellings by 95.1±2.6%, in comparison to $Sp^{A/A}$ neurons treated with DMSO (reduction of 4.15±4%, $p<0.001$; Fig. 5A a-d, B). Indeed, means of 6.8±0.6, 6.4±0.3 and 0.5±0.2 axonal swellings per 100 nuclei were respectively obtained for untreated, DMSO-treated and 100 nM nocodazole-treated $Sp^{A/A}$ neurons. Moreover, the treatment of $Sp^{A/A}$ DIV5 neurons with 10 nM vinblastine or 10 nM taxol also decreases the swelling number by 88.5±1.14% and 67±5.08% respectively, compared to the DMSO-treated control neurons (1±0,2%, $p\leq0.001$; Fig. 5A c, e-f, B). Means of 6.6±0.4, 6.5±0.7, 0.8±0.2 and 2.2±0.3 axonal swellings per 100 nuclei were respectively obtained for untreated, DMSO, 10 nM vinblastin and 10 nM taxol-treated $Sp^{A/A}$ neurons. Each set of experiments was reproduced three times independently. Because of the well-established role of microtubule dynamics in axon outgrowth, we assessed the effect of each drug treatment on neurite density. Importantly, neurite outgrowth was not affected when DIV5 $Sp^{A/A}$ cortical neurons were treated with 100 nM nocodazole, 10 nM vinblastine or 10 nM taxol compared with untreated or DMSO-treated neurons (data not shown). To explore whether an earlier treatment could similarly prevent the formation of axonal swellings, we

treated mutant cortical neurons with 50 nM nocodazole at DIV2. Interestingly, the treatment at DIV2 equally abolished the formation of neurite swellings but significantly affected neurite outgrowth (Fig. S3).

Altogether, our data show that axonal swellings of spastin-deficient neurons result from a defect in the regulation of microtubule dynamics in cortical axons. Importantly, substoichiometric concentrations of microtubule-targeting drugs are able to rescue the main pathological phenotype of $Sp^{\Delta/\Delta}$ mutant cortical neurons at DIV5, without affecting neurite density or neuron survival.

Discussion

The goal of this study was to tackle the molecular mechanisms responsible for the phenotype of spastin knockout mutant mice using primary cultures of cortical neurons. We here provide compelling evidence that the lack of mouse spastin leads to abnormal stabilization and organization of the microtubule network along cortical axons associated with the occurrence of swellings. This abnormal stabilization of the microtubule network in $Sp^{\Delta/\Delta}$ cortical neurons is consistent with previous studies in *Drosophila* showing that the knockdown of D-spastin equally causes an increased stabilization of the microtubule network at the neuromuscular junction associated with synaptic growth and neurotransmission defects (Trotta *et al,.* 2004; Orso *et al.,* 2005). Since alterations of microtubule dynamics are also observed in $Sp^{\Delta/\Delta}$ non-swollen axons and that microtubule-targeting drugs prevent the occurrence of axonal swellings in mutant cortical neurons, our data strongly suggest that misregulation of microtubule dynamics is a primary event in the axonopathy of our mouse mutant and thereby in the pathogenesis of *SPG4*-linked HSP.

Based on the well-characterized role of spastin in microtubule severing (Evans *et al.*, 2005; White *et al.*, 2007), we propose that the abnormal dynamics of microtubules results from the loss of spastin microtubule-severing activity. Recent studies have shown that spastin preferentially severs microtubules harboring specific post-translational modifications of their C-terminal tail (Roll-Mecak and Vale, 2008, Lacroix *et al.*, 2010). For example, the use of an antibody against the exposed glutamate residues on tubulin C-terminal tail totally inhibits spastin-mediated severing whereas such inhibition never occurs with an antibody directed against tyrosinated residues located in the same region (Roll-Mecak and Vale, 2008). Furthermore, spastin overexpression in neurons preferentially disrupts detyrosinated (Glu-tubulin) and acetylated (i.e., stable microtubules) rather than tyrosinated microtubules (i.e., dynamic microtubules, Riano *et al.*, 2009) demonstrating that spastin selectively severs

specific subpopulations of microtubules. Accordingly, we previously showed that the lack of spastin microtubule-severing activity in knock-out mice induces an accumulation of detyrosinated and delta 2-tubulin, two markers of stable microtubules, within axonal swellings of $Sp^{\Delta/\Delta}$ cortical neurons (Tarrade *et al.*, 2006). Moreover, we have here established that spastin loss of function strikingly decreases the number of dynamic microtubule plus ends within the axon shaft of cortical neurons. Importantly, spastin knockdown was similarly shown to reduce the number of microtubules plus ends in zebrafish developing neurons (Butler *et al.,* 2010) while its overexpression was reported to increase the number of EB3 comets in rat hippocampal neurons (Qiang *et al.,* 2010). Altogether, these results suggest that spastin loss of function would lead to the formation of longer and "long-lived" microtubules that are potentially submitted to various post-translational modifications (such as detyrosination and acetylation), which can influence the recruitment of microtubule-associated proteins (MAP) and therefore change the dynamic properties of these polymers. For exemple, it has been shown that long-lived detyrosinated microtubules become less susceptible to the depolymerizing activity of the molecular motor Kinesin 13 (Peris *et al.,* 2009), which additionally increases microtubule stability. Long-lived microtubules could also be recognized by microtubule-stabilizing proteins (like Tau and MAP1B), further enhancing their stability. This paradigm is supported by the local accumulation of Tau in axonal swellings of spastin-deficient cortical neurons (Kasher *et al.,* 2009 and present study).

Furthermore, several studies showed that the increased density of MAP along microtubules significantly impairs plus-end-directed microtubule transport by reducing the frequency of interaction between kinesin and microtubules (for review, see Baas and Qiang, 2005). The increased stability of the microtubule network caused by spastin depletion may thus be primarily responsible for the impaired anterograde axonal transport of mitochondria and organelles described in non-swollen $Spast^{\Delta E7/\Delta E7}$ cortical axons from another mutant

mouse (Kasher *et al.,* 2009). Interestingly, while anterograde transport is affected all along *Spast*$^{\Delta E7/\Delta E7}$ axons (Kasher *et al*., 2009), we and others have described a specific alteration of retrograde axonal transport in the distal part of both *Spast*$^{\Delta E7/\Delta E7}$ and *Sp*$^{\Delta/\Delta}$ cortical axons (Kasher *et al.*, 2009; present study). Intriguingly, although the axonal swellings of *Spast*$^{\Delta E7/\Delta E7}$ mice are morphologically similar to those observed in the spinal cord of our *Sp*$^{\Delta/\Delta}$ mice, *Spast*$^{\Delta E7/\Delta E7}$ axonal swellings are stochastically distributed along the axons of cultured neurons (Kasher *et al.*, 2009), whereas axonal swellings only occur in the distal part of *Sp*$^{\Delta/\Delta}$ axons in our cultures (Tarrade *et al.*, 2006). The discrepancy between these two mouse models might be either due to different genetic background or to diverse experimental conditions used for primary cultures of neurons.

In our model, the specific localization of the swellings in the distal region of the axon suggests a higher sensitivity of this area to the lack of spastin microtubule-severing activity and therefore provides a potential explanation for the dying-back axonopathy in *SPG4*-linked HSP. This increased sensitivity may be explained by spastin enrichment in the distal portion of the axons in normal conditions (Errico *et al*., 2004; Yu *et al*., 2008) but can also be generated by the lack of a highly specialized function of spastin in this particular region. Since loss of spastin causes alterations of both microtubule dynamics and retrograde axonal transport in this region, we propose that spastin could participate to the local coupling of microtubule severing and axonal transport. Using live imaging, we show that the vesicles located within axonal swellings display Brownian motion that is reminiscent of that described for microtubule-uncharged cargoes, and that the local accumulation of organelles at the swelling proximal region results from delayed and impaired transport rather than from a complete obstruction of retrograde axonal transport. Our results therefore suggest that spastin depletion may locally alter cargo loading onto microtubules. Interestingly, tubulin post-translational modifications were shown to influence the recruitment of protein complexes

such as MAPs (i.e., Tau, MAP1B) or plus-end tracking proteins ($p150^{Glued}$, EB1, CLIP170) onto microtubules (Verhey *et al.*, 2007). In primary cultures of mouse fibroblasts and neurons from TTL (Tubulin Tyrosine Ligase) knock-out mice, the accumulation of detyrosinated tubulin leads to the abnormal localization of the CAP-Gly plus-end-tracking proteins (+TIPs) such as $p150^{Glued}$, a member of the dynein complex, and CLIP170 (Peris *et al.*, 2006). As $p150^{Glued}$ has a critical role in cargo loading and microtubule retrograde transport (Vaughan *et al.*, 2002) and CLIP in linking organelle membranes to microtubules (Pierre *et al.,* 1992; Rickard and Kreis, 1996), we propose that the accumulation of detyrosinated-tubulin within $Sp^{\Delta/\Delta}$ axonal swellings may affect the recruitment of these +TIPs to microtubule plus ends and thereby the efficiency of retrograde axonal transport. This hypothesis leads us to propose a model in which spastin microtubule-severing activity would create novel microtubule plus ends, in the distal part of the axons, that are used as local nucleation points for the synthesis of tyrosinated dynamic microtubules as well as for $p150^{Glued}$ and CLIP cargo loading onto microtubules (Fig.7A). Alterations of spastin function might thus decrease dynamic microtubule plus ends (present study and Butler *et al.,* 2010), which would dampen microtubule dynamics as well as cargo loading onto microtubules and thereby axonal transport (Fig.7B).

Interestingly, neuropathological studies of patients with *SPG4*-linked HSP revealed the presence of axonal swellings in the corticospinal tracts and posterior columns (Kasher *et al.*, 2009). This observation indicates that the pathogenic mechanisms responsible for the axonopathy in the spastin knock-out mice (Tarrade *et al.*, 2006; Kasher *et al.*, 2009) seem to be conserved in the human disease and that the two existing mouse models are thus particularly relevant to study the physiopathology of *SPG4*-linked HSP.

Finally, we show that nanomolar concentrations of microtubule targeting-drugs, such as nocodazole, vinblastine or taxol alleviate the main pathological feature of spastin-depleted

cortical neurons by dramatically reducing the number of axon swellings. Our findings corroborate a previous analysis in *Drosophila*, which showed that the treatment of spastin-depleted larvae with low doses of vinblastine (i.e., 5 nM) significantly attenuates the pathological phenotype associated with either D-spastin knockdown or overexpression of a mutated (K467R) D-spastin (Orso *et al.*, 2005). Our analysis thus reveals that the pathogenic processes generated by spastin loss-of-function, which could be similarly rescued in *Drosophila* and mouse models, are highly conserved between invertebrates and vertebrates. Although high concentrations of nocodazole and vinblastine destabilize microtubules whereas taxol stabilizes microtubules at high doses, low and substoichiometric concentrations of each of these three compounds, as used in the present study, have the same effect and dampen microtubule dynamic instability without a significant impact on microtubule mass (for review, see Jordan and Wilson, 2004; Jordan and Wilson, 1990; Jordan *et al.*, 1991; Toso *et al.*, 1993; Jordan *et al.*, 1993; Tanaka *et al.*, 1995; Vasquez *et al.*, 1997). This paradigm thus implies that in our experimental conditions, these low doses of taxol would not further enhance the whole microtubular mass stability, which would have worsened the phenotype of mutant cortical axons, but may instead prevent the formation of axonal swellings by locally restraining microtubule dynamic instability at the end of axons, with minimal effect on microtubule structural integrity. Importantly, treatments of *Aplysia* bag cell neurons with similar doses of taxol and vinblastine to those we used here resulted in the same effect on growing axons *in vitro*. Indeed, at these nanomolar concentrations, both drugs suppress microtubule extension during growth cone steering and turning by dampening microtubule dynamics (Suter *et al*., 2004). Using videomicroscopy, Suter *et al.* (2004) could demonstrate that taxol or vinblastine application causes microtubules to undergo long pauses in their assembly, which subsequently blocks microtubule advance within the growth cone. Similarly, low doses of nocodazole, taxol or vinblastine may prevent the formation of novel axonal

swellings in $Sp^{4/4}$ cortical neurons by blocking microtubule assembly in the distal region of the axon.

In conclusion, our analysis shows that a modulation of microtubule dynamics using different microtubule-targeting drugs can efficiently reduce the occurrence of axonal swellings in mammalian spastin-deficient neurons. Although the molecular bases underlying the rescue of $Sp^{4/4}$ neurons by these drugs need to be further dissected, our results provide new insights into potential suppressors of the early axonal phenotype in mammalian models of HSP, which may orientate future development of therapeutic strategies.

Methods

Antibodies

The following primary antibodies were used: acetylated α-tubulin (clone 6-11B-1, Sigma), actin (clone AC-40, Sigma), EEA1 (clone 14, BD Transduction Laboratories), Lamp-1 (clone 1D4B, PharMingen), snap23a (G-16, Santa Cruz Biotechnology), β-III tubulin (TUJ-1, Covance), Tau-1 (clone PC1C6, Millipore), delta 2-tubulin (kindly provided by A. Andrieux), phospho-NF 200 (SMI 31, Chemicon), Caspase 3 (R&D systems), GFP (Invitrogen) and the S51 rabbit polyclonal antiserum against spastin (kindly provided by E. Rugarli; Errico *et al.*, 2004).

Western Blot analysis

Immunoblots were performed using 10 to 40µg of total brain protein extracts from 4 month-old $Sp^{+/+}$, $Sp^{\Delta/+}$, $Sp^{\Delta/\Delta}$ mice (Tarrade *et al.,* 2006) or 5 µg of total protein lysate from Cos-7 mock cells or cells transfected with *GFP-*Sp^{+} or *GFP-*Sp^{Δ} (Tarrade *et al,*. 2006). Protein extracts were prepared using an SDS-lysis buffer (25 mM sodium sulfate pH 7.2, 5 mM EDTA, 1% SDS) supplemented with 1 mM PMSF and a cocktail of protease inhibitors (Roche), and dosed with a BCA assay. The extracts were electrophoresed on 10% SDS-PAGE and transferred onto nitrocellulose membranes. Membranes were incubated overnight at 4°C with spastin polyclonal antiserum S51 (1:1000), anti-GFP polyclonal antibody (1:6000) or anti-actin monoclonal antibody (1:10,000). After several washes in PBS-T buffer (PBS, 0.05% Tween 20), membranes were incubated for one hour at room temperature with peroxydase-labeled goat anti-rabbit or anti-mouse antibodies (Santa Cruz Biotechnology). Immunostained proteins were visualized using enhanced chemiluminescence detection system (Santa Cruz Biotechnology). Spastin levels from 4 month-old $Sp^{+/+}$, $Sp^{\Delta/+}$ and $Sp^{\Delta/\Delta}$ mouse brain extracts were estimated by quantifying the immunoblot band density normalized to actin

values (Image J software) in three independent experiments. Values were statistically compared using an unpaired t test (Statview software).

Primary cultures of cortical and hippocampal neurons

Primary cultures of cortical neurons were prepared from 14.5 d.p.c. $Sp^{+/+}$ and $Sp^{\Delta/\Delta}$ embryos as described previously (Tarrade *et al.*, 2006). Primary cultures of hippocampal neurons were prepared from 17.5 d.p.c. $Sp^{+/+}$ and $Sp^{\Delta/\Delta}$ embryos. Hippocampi were dissected in Mg^{2+}, Ca^{2+}-free HBSS, and incubated with trypsin (0.25% trypsin in Mg^{2+}, Ca^{2+}-free HBSS) for 20 minutes at 37°C. Hippocampi were then washed three times in Mg^{2+}, Ca^{2+}-free HBSS and mechanically dissociated by repeated triturations in Neurobasal medium (Invitrogen) supplemented with 2% of B27 (Invitrogen). Hippocampal neurons were plated as previously described for cortical neurons (Tarrade *et al.*, 2006). Cells were maintained for six or twelve days at 37°C in 5% CO_2. The assessment of neurite outgrowth was performed using a stereological method as previously reported (Ronn *et al.*, 2000). All animal procedures were performed in accordance with institutional guidelines (agreement B91-228-2 and 3429).

Retrograde labeling experiments

Retrograde axonal transport was analyzed in $Sp^{+/+}$ and $Sp^{\Delta/\Delta}$ cortical neurons using the neuronal retrograde tracer cholera toxin B (CTb) conjugated with Alexa fluor 488 (Molecular Probes). Six days after plating, $Sp^{+/+}$ and $Sp^{\Delta/\Delta}$ neurons were incubated with 1 µg/mL of CTb Alexa Fluor 488 for 15 min at 37°C in Neurobasal medium plus B27 and washed in CTb-free medium for 30 min or 3 h. Cortical neurons were fixed with 2% paraformaldehyde in 1X phosphate-buffered saline (PBS) supplemented with 0.16 M sucrose for 10 minutes at 37°C. Cells were processed for immunolabeling of acetylated α-tubulin or actin and mounted with Vectashield and Dapi for observation. For each experimental condition, we analyzed more

than 100 neurons and scored the percentage of soma showing an accumulation of CTb. Control and mutant scores were statistically compared using an unpaired t test (Statview software).

Time-lapse video microscopy

For phase-contrast video microscopy, DIV6 $Sp^{\Delta/\Delta}$ cortical neurons were placed in a chamber at 37°C under 5% of CO2. Individual axonal swelling was imaged using an Axiophot microcoscope (Zeiss). The movie is composed of 500-ms stills taken every 30 seconds over a period of 9 hours. To visualize microtubule plus-end dynamics, $Sp^{+/+}$and $Sp^{\Delta/\Delta}$ cortical neurons were transfected before plating with 1μg of DNA (EB3-GFP; kindly provided by F. Nothias), using the Nucleofector apparatus and the Basic Nucleofector Kit for primary mammalian neurons (Lonza). Time-lapse recording of EB3-GFP comets were performed at 37°C on DIV6 $Sp^{+/+}$and $Sp^{\Delta/\Delta}$ transfected cortical neurons using a Leica DMI 6000B inverted spinning disk microscope with a 63x immersion objective. Images were acquired every 2 seconds over a period of 10 minutes. A minimal total of 20 axons were analyzed per genotype. Comet velocity and number were estimated using Kymograph analysis (yt, images; Fiji software), with lines drawn along the axon. Kymograph production and analysis were automated using a Fiji macro designed and written by P. Mailly. Statistical analyses were performed using the Student's t test (Statview software). Kymographs of swollen axons were generated by analyzing the behavior of EB3-GFP comets in the whole volume of the swellings using the same method.

Electron microscopy

Primary cultures of DIV6 cortical neurons were fixed with 4% paraformaldehyde and 3% glutaraldehyde in 0.1 M phosphate buffer (pH 7.4) and processed for electron microscopy as

described previously (Tarrade *et al*., 2006; Frugier *et al.*, 2000). Ultrathin sections were stained with uranyl acetate and lead citrate, and examined with a Tecnai F20 transmission electron microscope (Philips) at 200 kV.

Nocodazole susceptibility assay

Cultured $Sp^{+/+}$ and $Sp^{\Delta/\Delta}$ cortical neurons were treated with 30 µM nocodazole (Sigma) in DMSO or with DMSO alone for 40 min, permeabilized in PHEM buffer (60 mM Pipes, 25 mM Hepes, 10 mM EGTA, and 2 mM MgCl2, pH 6.9) with 0.02% saponin and 10 µM taxol, and fixed in PHEM buffer with 2% paraformaldehyde and 0.05% glutaraldehyde. The whole microtubule network was analyzed using a ßIII-tubulin antibody and cell morphology was visualized by actin filament immunostaining with phalloidin. Moreover, we carried out another set of experiments in which, $Sp^{\Delta/\Delta}$ cortical neurons were treated with 40 µM nocodazole for 0, 30, 60 or 90 minutes before fixation.

Pharmacological treatment of cortical neurons

Primary cultures of $Sp^{+/+}$ and $Sp^{\Delta/\Delta}$ cortical neurons were treated 2 or 5 days after plating with either 50 or 100 nM nocodazole, 10 nM vinblastine (Sigma), 10 nM taxol (Sigma) or DMSO (as a control) in Neurobasal medium supplemented with 2% B27. Six days after plating, cortical neurons were fixed with 2% paraformaldehyde/0.16 M sucrose in PBS for 10 minutes at 37°C, processed through immunolabeling of acetylated α-tubulin and mounted with Vectashield and Dapi. The number of neurite swellings per 100 nuclei was determined for each condition and scores were statistically compared using an unpaired t test (Statview software). Each set of experiments was reproduced 3 times independently and more than 1000 neurons were analyzed per experiment.

Immunocytochemistry

After several washes in PBS, cells were fixed with 2% paraformaldehyde/0.16 M sucrose for 10 minutes at 37°C, permeabilized with 0.1% Triton X-100 in PBS for 5 minutes and left in blocking reagent (3% BSA/5% normal goat or donkey serum in PBS) for one hour at room temperature. Primary antibodies were diluted to the appropriate concentrations in the blocking reagent and incubated with cells overnight at 4°C. Cells were subsequently washed 4 times with PBS, incubated one hour at room temperature with the appropriate secondary antibodies and washed again in PBS. Cells were mounted with vectashield and Dapi and observed with an epifluorescence microscope (Zeiss Axophot).

ACKNOWLEDGEMENTS

We are grateful to Elena Rugarli and Annie Andrieux for providing us with spastin and delta-2 tubulin antibodies respectively. We thank Alain Thorel and Mohamed Sennour (Centre des Matériaux, Ecole des Mines, Evry, France) for their help in electron microscopy, and Richard Schwartzmann from the Cell Imaging and Flow Cytometry facility of the IFR83 (Paris, France) for his precious help in time-lapse videomicroscopy of EB3-GFP comets. The IFR83 facility is supported by the Conseil regional d'Ile-de-France. We also thank the SPATAX network for helpful discussions and Genopole (Evry) for constant support to P.A.C. This work was supported by INSERM, the Fédération pour la Recherche sur le Cerveau, GIS-ANR Maladies Rares, Université d'Evry and the Conseil Régional d'Ile de France to J.M.

CONFLICT OF INTEREST STATEMENT

The authors have no conflicting financial interests.

AUTHOR CONTRIBUTIONS

JM and CF conceived the project and designed the experiments. CF, AT and LP performed all experiments, and analyzed the data together with JM. SC, PM, CD, SD and NR provided technical assistance. PC and DJ supervised AT and LP in their respective labs and had insightful comments on the project. CF, JH, LP and JM wrote the manuscript.

REFERENCES

Baas, P.W., Karabay, A. and Qiang, L. (2005). Microtubules cut and run. *Trends Cell Biol.* **15**, 518-524.

Baas, P.W. and Qiang, L. (2005). Neuronal microtubules: when the MAP is the roadblock. *Trends Cell Biol.* **15**, 183-187.

Blackstone, C., O'Kane, C.J. and Reid E. (2011). Hereditary spastic paraplegias: membrane traffic and the motor pathway. *Nat. Rev. Neurosci.* **12**, 31-42.

Butler, R., Wood, J.D., Landers, J.A. and Cunliffe, V.T. (2010). Genetic and chemical modulation of spastin-dependent axon outgrowth in zebrafish embryos indicates a role for impaired microtubule dynamics in hereditary spastic paraplegia. *Dis. Model Mech.* **3**, 743-751.

Cashman, N.R., Durham, H.D., Blusztajn, J.K., Oda, K., Tabira, T., Shaw, I.T., Dahrouge, S. and Antel, J.P. (1992). Neuroblastoma x spinal cord (NSC) hybrid cell lines resemble developing motor neurons. *Dev. Dyn.* **194**, 209-221.

Charvin, D., Cifuentes-Diaz, C., Fonknechten, N., Joshi, V., Hazan, J., Melki, J. and Betuing, S. (2003). Mutations of SPG4 are responsible for a loss of function of spastin, an abundant neuronal protein localized in the nucleus. *Hum. Mol. Genet.* **12**, 71-78.

Claudiani, P., Riano, E., Errico, A., Andolfi, G. and Rugarli, E.I. (2005). Spastin subcellular localization is regulated through usage of different translation start sites and active export from the nucleus. *Exp. Cell Res.* **309**, 358-369.

Connell, J.W., Lindon, C., Luzio, J.P. and Reid, E. (2009). Spastin couples microtubule severing to membrane traffic in completion of cytokinesis and secretion. *Traffic* **10**, 42-56.

Depienne, C., Fedirko, E., Forlani, S., Cazeneuve, C., Ribaï, P., Feki, I., Tallaksen, C., Nguyen, K., Stankoff, B., Ruberg, M., Stevanin, G., Dürr, A. and Brice, A. (2007).

Exon deletions of SPG4 are a frequent cause of hereditary spastic paraplegia. *J. Med. Genet.* **44**, 281-284.

Du, F., Ozdowski, E.F., Kotowski, I.K., Marchuk, D.A. and Sherwood, N.T. (2010). Functional conservation of human Spastin in a Drosophila model of autosomal dominant-hereditary spastic paraplegia. *Hum. Mol. Genet*. **19**, 1883-1896.

Errico, A., Ballabio, A. and Rugarli, E.I. (2002). Spastin, the protein mutated in autosomal dominant hereditary spastic paraplegia, is involved in microtubule dynamics. *Hum. Mol. Genet.* **11**, 153-163.

Errico, A., Claudiani, P., D'Addio, M. and Rugarli, E.I. (2004). Spastin interacts with the centrosomal protein NA14, and is enriched in the spindle pole, the midbody and the distal axon. *Hum. Mol. Genet.* **13**, 2121-2132.

Evans, K.J., Gomes, E.R., Reisenweber, S.M., Gundersen, G.G. and Lauring, B.P. (2005). Linking axonal degeneration to microtubule remodeling by Spastin-mediated microtubule severing. *J. Cell Biol.* **168**, 599-606.

Fink, J.K. (2006). Hereditary spastic paraplegia. *Curr. Neurol. Neurosci. Rep.* **6**, 65-76.

Fonknechten, N., Mavel, D., Byrne, P., Davoine, C.S., Cruaud, C., Bönsch, D., Samson, D., Coutinho, P., Hutchinson, M., McMonagle, P., Burgunder, J.M., Tartaglione, A., Heinzlef, O., Feki, I., Deufel, T., Parfrey, N., Brice, A., Fontaine, B., Prud'homme, J.F., Weissenbach, J., Dürr, A. and Hazan, J. (2000). Spectrum of *SPG4* mutations in autosomal dominant spastic paraplegia. *Hum. Mol. Genet.* **9**, 637-644.

Frugier, T., Tiziano, F.D., Cifuentes-Diaz, C., Miniou, P., Roblot, N., Dierich, A., Le Meur, M. and Melki J. (2000). Nuclear targeting defect of SMN lacking the C-terminus in a mouse model of spinal muscular atrophy. *Hum. Mol. Genet.* **9**, 849-858.

Gundersen, G.G., Kalnoski, M.H. and Bulinski, J.C. (1984). Distinct populations of microtubules: tyrosinated and nontyrosinated alpha tubulin are distributed differently in vivo. *Cell*. **38**, 779-789.

Hazan, J., Fonknechten, N., Mavel, D., Paternotte, C., Samson, D., Artiguenave, F., Davoine, C.S., Cruaud, C., Dürr, A., Wincker, P., Brottier, P., Cattolico, L., Barbe, V., Burgunder, J.M., Prud'homme, J.F., Brice, A., Fontaine, B., Heilig, R. and Weissenbach, J. (1999). Spastin, a new AAA protein, is altered in the most frequent form of autosomal dominant spastic paraplegia. *Nat. Genet.* **23**, 296-303.

Jordan, M.A. and Wilson, L. (1990). Kinetic analysis of tubulin exchange at microtubule ends at low vinblastine concentrations. *Biochemistry* **29**, 2730-2739.

Jordan, M.A., Thrower, D. and Wilson, L. (1991). Mechanism of inhibition of cell proliferation by Vinca alkaloids. *Cancer Res.* **51**, 2212-2222.

Jordan, M.A., Toso, R.J., Thrower, D. and Wilson, L. (1993). Mechanism of mitotic block and inhibition of cell proliferation by taxol at low concentrations. *Proc. Natl. Acad. Sci. USA* **90**, 9552-9556.

Jordan, M.A. and Wilson, L. (2004). Microtubules as a target for anticancer drugs. *Nat. Rev. Cancer* **4**, 253-265.

Karabay, A., Yu, W., Solowska, J.M., Baird, D.H. and Baas, P.W. (2004). Axonal growth is sensitive to the levels of katanin, a protein that severs microtubules. *J. Neurosci.* **24**, 5778-5788.

Kasher, P.R., De Vos, K.J., Wharton, S.B., Manser, C., Bennett, E.J., Bingley, M., Wood, J.D., Milner, R., McDermott, C.J., Miller, C.C., Shaw, P.J. and Grierson, A.J. (2009). Direct evidence for axonal transport defects in a novel mouse model of mutant spastin-induced hereditary spastic paraplegia (HSP) and human HSP patients. *J. Neurochem.* **110**, 34-44.

Lacroix, B., Van Dijk, J., Gold, N.D., Guizetti, J., Aldrian-Herrada, G., Rogowski, K., Gerlich, D.W. and Janke, C. (2010). Tubulin polyglutamylation stimulates spastin-mediated microtubule severing. *J. Cell Biol.* **189**, 945-954.

Lencer, W.I., Hirst, T.R. and Holmes, R.K. (1999). Membrane traffic and the cellular uptake of cholera toxin. *Biochim. Biophys. Acta* **1450**, 177-190.

Lumb JH, Connell JW, Allison R and Reid E. (2012). The AAA ATPase spastin links microtubule severing to membrane modelling. *Biochim Biophys Acta.* **1823**, 192-197.

Ma, D.L., Chia, S.C., Tang, Y.C., Chang, M.L., Probst, A., Burgunder, J.M. and Tang, F.R. (2006). Spastin in the human and mouse central nervous system with special reference to its expression in the hippocampus of mouse pilocarpine model of status epilepticus and temporal lobe epilepsy. *Neurochem. Int.* **49**, 651-664.

Orso, G., Martinuzzi, A., Rossetto, M.G., Sartori, E., Feany, M. and Daga, A. (2005). Disease-related phenotypes in a Drosophila model of hereditary spastic paraplegia are ameliorated by treatment with vinblastine. *J. Clin. Invest.* **115**, 3026-3034.

Park, S.H., Zhu, P.P., Parker, R.L. and Blackstone, C. (2010). Hereditary spastic paraplegia proteins REEP1, spastin and atlastin-1 coordinate microtubule interactions with the tubular ER network. *J. Clin. Invest.* **120**, 1097-1110.

Paturle-Lafanechère L, Manier M, Trigault N, Pirollet F, Mazarguil H and Job D. (1994). Accumulation of delta 2-tubulin, a major tubulin variant that cannot be tyrosinated, in neuronal tissues and in stable microtubule assemblies. *J Cell Sci.* **107**, 1529-1543.

Peris, L., Thery, M., Fauré, J., Saoudi, Y., Lafanechère, L., Chilton, J.K., Gordon-Weeks, P., Galjart, N., Bornens, M., Wordeman, L., Wehland, J., Andrieux, A. and Job, D. (2006). Tubulin tyrosination is a major factor affecting the recruitment of CAP-Gly proteins at microtubule plus ends. *J. Cell Biol.* **174**, 839-849.

Peris, L., Wagenbach, M., Lafanechère, L., Brocard, J., Moore, A.T., Kozielski, F., Job, D., Wordeman, L. and Andrieux, A. (2009). Motor-dependent microtubule disassembly driven by tubulin tyrosination. *J Cell Biol.* **185**, 1159-1166.

Pierre, P., Scheel, J., Rickard, J.E. and Kreis T.E. (1992). CLIP-170 links endocytic vesicles to microtubules. *Cell.* **70**, 887-900.

Qiang L, Yu W, Liu M, Solowska J.M and Baas P.W. (2010). Basic fibroblast growth factor elicits formation of interstitial axonal branches via enhanced severing of microtubules. *Mol Biol Cell*. **21**, 334-344.

Reid, E. (2003). Science in motion: common molecular pathological themes emerge in the hereditary spastic paraplegias. *J. Med. Genet.* **40**, 81-86.

Riano, E., Martignoni, M., Mancuso, G., Cartelli, D., Crippa, F., Toldo, I., Siciliano, G., Di Bella, D., Taroni, F., Bassi, M.T., Cappelletti, G. and Rugarli, E.I. (2009). Pleiotropic effects of spastin on neurite growth depending on expression levels. *J. Neurochem*. **108**, 1277-1288.

Rickard, J.E. and Kreis, T.E. (1996). CLIPs for organelle-microtubule interactions. *Trends Cell Biol*. **6**, 178-183.

Roll-Mecak, A. and Vale, R.D. (2005). The Drosophila homologue of the hereditary spastic paraplegia protein, spastin, severs and disassembles microtubules. *Curr. Biol.* **15**, 650-655.

Roll-Mecak, A. and Vale, R.D. (2008). Structural basis of microtubule severing by the hereditary spastic paraplegia protein spastin. *Nature* **451**, 363–367.

Ronn, L.C., Ralets, I., Hartz, B.P., Bech, M., Berezin, A., Berezin, V., Moller, A. and Bock, E. (2000). A simple procedure for quantification of neurite outgrowth based on stereological principles. *J. Neurosci. Methods* **100**, 25-32.

Salinas, S., Carazo-Salas, R.E., Proukakis, C., Cooper, J.M., Weston, A.E., Schiavo, G. and Warner, T.T. (2005). Human spastin has multiple microtubule-related functions. *J. Neurochem.* **95**, 1411–1420.

Salinas, S., Proukakis, C., Crosby, A. and Warner, T.T. (2008). Hereditary spastic paraplegia: clinical features and pathogenic mechanisms. *Lancet Neurol*. **7**, 1127-1138.

Sherwood, N.T., Sun, Q., Xue, M., Zhang, B. and Zinn, K. (2004). Drosophila spastin regulates synaptic microtubule networks and is required for normal motor function. *PLoS Biol.* **2**, 2094-2111.

Solowska, J.M., Morfini, G., Falnikar, A., Himes, B.T., Brady, S.T., Huang, D. and Baas, P.W. (2008). Quantitative and functional analyses of spastin in the nervous system: implications for hereditary spastic paraplegia. *J. Neurosci.* **28**, 2147-2157.

Solowska, J.M., Garbern, J.Y. and Baas, P.W. (2010). Evaluation of loss of function as an explanation for SPG4-based hereditary spastic paraplegia. *Hum. Mol. Genet*. **19**, 2767-2779.

Stepanova T, Slemmer J, Hoogenraad CC, Lansbergen G, Dortland B, De Zeeuw CI, Grosveld F, van Cappellen G, Akhmanova A and Galjart N.J. (2003). Visualization of microtubule growth in cultured neurons via the use of EB3-GFP (end-binding protein 3-green fluorescent protein). *J Neurosci*. **23**, 2655-2664.

Suter, D.M., Schaefer, A.W. and Forscher, P. (2004). Microtubule dynamics are necessary for Src family kinase-dependent growth cone steering. *Curr. Biol.* **14**, 1194-1199.

Tanaka, E., Ho, T. and Kirschner, M.W. (1995). The role of microtubule dynamics in growth cone motility and axonal growth. *J. Cell Biol.* **128**, 139-155.

Tarrade, A., Fassier, C., Courageot, S., Charvin, D., Vitte, J., Peris, L., Thorel, A., Mouisel, E., Fonknechten, N., Roblot, N., Seilhean, D., Diérich, A., Hauw, J.J. and Melki, J. (2006). A mutation of spastin is responsible for swellings and impairment of transport

in a region of axon characterized by changes in microtubule composition. *Hum. Mol. Genet.* **15**, 3544–3558.

Toso, R.J., Jordan, M.A., Farrell, K.W., Matsumoto, B. and Wilson, L. (1993). Kinetic stabilization of microtubule dynamic instability in vitro by vinblastine. *Biochemistry* **32**, 1285-1293.

Trotta, N., Orso, G., Rossetto, M.G., Daga, A. and Broadie, K. (2004). The hereditary spastic paraplegia gene, spastin, regulates microtubule stability to modulate synaptic structure and function. *Curr. Biol.* **14**, 1135-1147.

Vasquez, R.J., Howell, B., Yvon, A.M., Wadsworth, P. and Cassimeris, L. (1997). Nanomolar concentrations of nocodazole alter microtubule dynamic instability in vivo and in vitro. *Mol. Biol. Cell.* **8**, 973-985.

Vaughan, P.S., Miura, P., Henderson, M., Byrne, B. and Vaughan, K.T. (2002). A role for regulated binding of p150 (Glued) to microtubule plus ends in organelle transport. *J. Cell Biol.* **158**, 305-319.

Verhey, K.J. and Gaertig, J. (2007). The tubulin code. *Cell Cycle* **6**, 2152-2160.

White, S.R., Evans, K.J., Lary, J., Cole, J.L. and Lauring, B. (2007). Recognition of C-terminal amino acids in tubulin by pore loops in spastin is important for microtubule severing. *J. Cell Biol.* **176**, 995–1005.

Wood, J.D., Landers, J.A., Bingley, M., McDermott, C.J., Thomas-McArthur, V., Gleadall, L.J., Shaw, P.J. and Cunliffe, V.T. (2006). The microtubule-severing protein spastin is essential for axon outgrowth in the zebrafish embryo. *Hum. Mol. Genet.* **15**, 2763-2771.

Yu, W., Qiang, L., Solowska, J.M., Karabay, A., Korulu, S. and Baas, P.W. (2008). The microtubule-severing proteins spastin and katanin participate differently in the formation of axonal branches. *Mol. Biol. Cell.* **19**, 1485-1498.

Legends to figures

Figure 1: Absence of truncated spastin in $Sp^{\Delta/\Delta}$ mutant mice. (**A**) Western blot analysis of protein extracted from non-transfected Cos-7 cells (NT) or transfected with constructs expressing *GFP-*Sp^{+} or *GFP-*Sp^{Δ} using S51 spastin polyclonal antibody (left panel) or GFP antibody (right panel). S51 antibody specifically recognizes the truncated spastin lacking its AAA domain (i.e., GFP-Sp^{Δ}), which is equally detected by the anti-GFP antibody. (**B**) Immunoblot analysis of spastin from 40µg (left panel) or 10µg (right panel) of 4 month-old $Sp^{+/+}$, $Sp^{\Delta/+}$ and $Sp^{\Delta/\Delta}$ brain lysates using S51 spastin antibody. $Sp^{\Delta/+}$ and $Sp^{\Delta/\Delta}$ brain lysates do not show any traces of truncated spastin. Note the reduction or complete absence of wild-type spastin isoforms in $Sp^{\Delta/+}$ and $Sp^{\Delta/\Delta}$ mice respectively. Actin was used as a loading control. (**C**) Quantification of spastin band density (including all spastin isoforms) normalized to actin values from three independent experiments. Spastin expression is reduced by 40% in $Sp^{\Delta/+}$ mice compared to $Sp^{+/+}$ mice ($p<0.05$) whereas no traces of wild-type spastin was detectable in $Sp^{\Delta/\Delta}$ mutants ($p<0.001$). A.U: Arbitrary Units. Vertical bars are standard errors.

Figure 2: Spastin deletion specifically affects the integrity of cortical axons. **(A-H)** Immunodetection of acetylated α-tubulin in primary cultures of DIV6 hippocampal **(**A, B, G, H**)** and cortical neurons (C, D, E, F) from $Sp^{+/+}$ (A, C) and $Sp^{\Delta/\Delta}$ (B, D, E-H) embryos. Unlike $Sp^{\Delta/\Delta}$ cortical neurons that show obvious axonal swellings (D, E, F; arrows), $Sp^{\Delta/\Delta}$ hippocampal neurons do not display any neurite swellings in the distal part of their axons (arrowheads) or in other regions of the axon (B, G, H). Neurite density was not affected in $Sp^{\Delta/\Delta}$ hippocampal neurons (B) compared to $Sp^{+/+}$ hippocampal neurons (A). Images (E-H) represent higher magnification of $Sp^{\Delta/\Delta}$ cortical (E, F) and hippocampal (G, H) axon distal regions. Scale bar: (A-D), 50 µm; (E-H), 20 µm. (**I**) Western blot analysis of spastin isoforms in protein lysates (20µg) from primary cultures of $Sp^{+/+}$ cortical and hippocampal neurons

using the S51 spastin antiserum. Actin was used as a loading control. H.N: Hippocampal Neurons, C.N: Cortical Neurons.

Figure 3: Ultrastructural analysis of $Sp^{\Delta/\Delta}$ cortical neurons reveals a massive disorganization of the microtubule network within axonal swellings. (**A-H**) Ultra-thin sections of DIV6 primary cultures of cortical neurons from $Sp^{\Delta/\Delta}$ (A-F) and $Sp^{+/+}$ mouse embryos (G-H). Images B and D are higher magnifications of axonal swellings indicated by arrows in images A and C respectively. Images (E, F and H) represent higher magnification of boxed regions in images (B), (D) and (G) respectively. Note the obvious disorganization and the tangled and bended aspect of microtubules within axonal swellings of $Sp^{\Delta/\Delta}$ cortical neurons (B, D, E and F). This abnormal appearance of microtubules was never observed in $Sp^{+/+}$ axons in which microtubules are always organized in parallel arrays (G-H). Scale bar: (A, C) 5μm; (B, D, G) 0.5μm; (E, F, H) 0.25μm.

Figure 4: Impaired microtubule disassembly in $Sp^{\Delta/\Delta}$ cultured cortical neurons. (A-L) $Sp^{+/+}$ (A-B, E-F) and $Sp^{\Delta/\Delta}$ (C-D, G-L) neurons 4 (A-H) or 6 days (I-L) post-plating. Neurons were incubated in the presence of 30 μM nocodazole for 40 min (E-H) or 40 μM nocodazole for 0 (I), 30 (J), 60 (K) or 90 min (L), then permeabilized in saponin-based buffer to extract free tubulin molecules and double-labeled for F-actin (red) and βIII-tubulin (green). After 40-minute exposure to 30 μM nocodazole, only a faint βIII-tubulin staining was still detectable in $Sp^{+/+}$ cortical axons (E) whereas a persistent microtubule signal was observed in $Sp^{\Delta/\Delta}$ axons (G). Note that the remaining microtubule signal was still present in $Sp^{\Delta/\Delta}$ axonal swellings after 90-minute exposure to 40 μM nocodazole, while only a residual labeling was observed in the other regions of the axon shaft (L). Scale bar: (A-H) 20μm; (I-L) 20μm.

Figure 5: Spastin loss of function decreases the number of dynamic microtubule plus ends in cortical axon shaft. (**A-E**) Time-lapse recording of EB3-GFP comets in DIV6 $Sp^{+/+}$ (n=20) and $Sp^{\Delta/\Delta}$ (n=29) cortical axons. (**A-B**) Kymographs of a $Sp^{+/+}$ (A) and $Sp^{\Delta/\Delta}$ (B) axon from a 10-minute time-lapse recording of EB3-GFP comets. These kymographs revealed a striking decrease of EB3-GFP moving comets in $Sp^{\Delta/\Delta}$ axon shaft, which is associated with a weak movement of diffuse EB3-GFP protein compared to $Sp^{+/+}$axon. Horizontal scale bar: 10μm; vertical scale bar: 2 minutes. (**C**) Quantification of the average number of EB3-GFP comets per 100 μm of axonal length. (**D**) Quantification of the mean EB3-GFP comet velocity. The average number of EB3-GFP comets is significantly reduced in $Sp^{\Delta/\Delta}$ axons compared to $Sp^{+/+}$ axons ($p<0.001$), whereas the mean comet speed is not affected by spastin depletion. Vertical bars are standard errors. (**E**) Kymograph analysis of microtubule plus ends (i.e., EB3-GFP comets) in a selected $Sp^{+/+}$ axonal region (left panel; Movie 2) and two distinct $Sp^{\Delta/\Delta}$ swollen axons (middle and right panels; Movies 4 and 5). The analyzed regions are boxed in Movies 2, 4 and 5 and are presented on the top of each kymograph. Kymographs showed that only very few EB3-GFP comets are moving within swellings and that the vast majority of these moving comets are located in the most distal end of the swelling. Horizontal scale bar: 5 μm; vertical scale bar: 2 minutes. P: proximal; D: distal. (A, B and E) Anterograde comets are represented by diagonal lines leading to the bottom right, while stationary comets (i.e., Fig. 5E right panel) are shown by vertical white lines.

Figure 6: Microtubule-targeting drugs rescue the pathological phenotype of $Sp^{\Delta/\Delta}$ cortical neurons. (**A**) Immunolabeling of acetylated α-tubulin on DIV6 primary cultures of $Sp^{+/+}$ (a) and $Sp^{\Delta/\Delta}$ (b-f) cortical neurons untreated (a, b) or treated 5 days post-plating with 100 nM of nocodazole (d), 10 nM of vinblastine (e), 10 nM of taxol (f) or the equivalent volume of DMSO (vehicule, c). Note the absence of axonal swellings in the distal region of $Sp^{\Delta/\Delta}$ cortical

neurons treated with microtubule-targeting drugs (d-f; arrowheads) compared with untreated or DMSO-treated $Sp^{\Delta/\Delta}$ neurons (arrows). The neurite morphology of mutant neurons treated with microtubule-targeting drugs appears similar to that of $Sp^{+/+}$ neurons (a). Scale bar: (a-f) 50μm. (**B**). The percentage of axonal swellings in $Sp^{\Delta/\Delta}$ cortical neuron cultures was evaluated at DIV6. Note that nanomolar concentrations of microtubule targeting-drugs significantly decrease the proportion of neurite swellings in primary cultures of $Sp^{\Delta/\Delta}$ neurons compared to DMSO-treated cultures. Asterisks indicate statistically different percentages between DMSO-treated neurons and 100 nM nocodazole ($p<0.001$), 10 nM vinblastine ($p<0.0001$) or 10 nM taxol ($p<0.0001$) -treated cells. Vertical bars indicate standard errors. (A-B) More than 1000 neurons were analyzed per experimental condition.

Figure 7: Hypothetical model of spastin function. Hypothetical model of spastin function in the distal part of cortical axons in physiological (A) and pathological (B) conditions. Cargoes that should be retrogradely transported are recruited on microtubule plus ends via the $p150^{Glued}$, a member of the dynactin complex. Then, the recruitment of the molecular motor dynein via $p150^{Glued}$ allows retrograde transport of cargoes to the soma along microtubules (Aa; Ba'). In the distal part of the axon, spastin severs microtubules to generate new microtubules plus ends (Ab) that may serve as local nucleation points for the synthesis of dynamic microtubules (Ac) and also improve retrograde axonal transport efficiency by increasing the number of microtubules plus ends, and thereby the capacity of cargo loading onto microtubules via $p150^{Glued}$ (Ac). In this region of the axon, loss of spastin microtubule-severing activity (Bb') might reduce the number of microtubule plus ends, that will subsequently affect both microtubule dynamics and cargo loading efficiency (Bc').

Figure S1: Retrograde axonal transport defect is not restricted to a subtype of organelles in $Sp^{\Delta/\Delta}$ neurons. (A-A'') Primary cultures of $Sp^{\Delta/\Delta}$ cortical neurons were incubated at DIV5, with 1μg/mL of the neuronal retrograde tracer Alexa488-conjugated CTb (A), washed in CTb-free medium, fixed and processed for immunolabeling with acetylated α-tubulin antibody (A', A''). Many CTb positive vesicles are accumulated within the proximal part of the swellings (A-A''; arrows). (B-D'') Co-immunolabeling of acetylated α-tubulin (tubulin; B', B'', C', C'', D' and D'') and endosomes (EEA1; B, B''), lysosomes (Lamp1; C, C''), synaptic vesicules (Snap23a; D, D'') in DIV6 primary cultures of $Sp^{\Delta/\Delta}$ cortical neurons. All these organelles are equally accumulated within axonal swellings (B-D''; arrows). (A- D'') Nuclei are stained with DAPI (asterisks). Panels (A''- D'') are higher magnifications of panels (A'- D'). Scale bars: 10 μm.

Figure S2: Excessive stabilization of microtubules in axonal swellings of $Sp^{\Delta/\Delta}$ cortical neurons. Primary cultures of DIV6 $Sp^{\Delta/\Delta}$ cortical neurons were immunolabeled for acetylated α-tubulin (A, C, D, F) and the microtubule-stabilizing protein Tau (Tau-1; B, C) or delta 2-tubulin, a marker of very long-lived microtubules (E, F). Insets show higher magnifications of axonal swellings. The accumulation of Tau and the two markers of long lived microtubules (aceylated α-tubulin and delta 2-tubulin) within the swellings strongly suggest that microtubules are abnormally stabilized in this axonal region. Scale bars: (A-F) 50μm; (insets) 10μm. (G-H) Quantitative fluorescence intensity profile of acetylated α-tubulin and Tau-1 (G) or acetylated α-tubulin and delta 2-tubulin (H) within and on either side of the swellings. Arrows indicate the proximal and distal parts of the swellings.

Figure S3: Nocodazole treatment at DIV2 prevents the formation of axonal swellings but affects $Sp^{\Delta/\Delta}$ cortical axon outgrowth. (A) Immunolabeling of acetylated α-tubulin on DIV6

primary cultures of $Sp^{+/+}$ (a-c) and $Sp^{\Delta/\Delta}$ (a'-c') cortical neurons untreated (a, a') or treated two days post-plating with 50 nM nocodazole (c, c') or with an equivalent volume of DMSO (b, b'). Note the absence of axonal swellings in the distal region of $Sp^{\Delta/\Delta}$ cortical neurons treated with nocodazole (c'; arrowheads) compared with untreated or DMSO-treated $Sp^{\Delta/\Delta}$ neurons (arrows). Scale bar: 50μm. (B). The percentage of axonal swellings in $Sp^{\Delta/\Delta}$ cortical neurons was evaluated at DIV6. Note that 50 nM nocodazole significantly decreases the proportion of neurite swellings in primary cultures of $Sp^{\Delta/\Delta}$ neurons compared to DMSO-treated cultures. Asterisks indicate statistically different percentages between DMSO-treated neurons and 50 nM nocodazole-treated cells (**P<0.001). Vertical bars indicate standard errors. (C). Analysis of neurite outgrowth at DIV6 in primary cultures of $Sp^{\Delta/\Delta}$ neurons treated with 50 nM nocodazole or with an equivalent volume of DMSO. The treatment of $Sp^{\Delta/\Delta}$ neurons with nocodazole at DIV2 dramatically and significantly affects neurite outgrowth compared with DMSO control treatment ($p<0.0001$). More than 1000 neurons were analyzed in each condition.

Movie 1: Impaired retrograde axonal transport in $Sp^{\Delta/\Delta}$ axonal swellings. Phase-contrast time-lapse videomicroscopy of a DIV6 $Sp^{\Delta/\Delta}$ neuron, focusing on axonal swellings. Note that spastin deletion does not abolish retrograde axonal transport but increases cargo stalling in the swelling resulting in their progressive accumulation (arrow).

Movie 2: Live imaging of dynamic microtubule plus ends in DIV6 $Sp^{+/+}$ cortical neurons expressing the EB3-GFP fusion protein. The movie is composed of 300 stills taken every 2 seconds over a period of 10 minutes. The axonal region used for kymograph analysis in the left panel of Fig. 5E is boxed.

Movie 3: Live imaging of dynamic microtubule plus ends in DIV6 $Sp^{\Delta/\Delta}$ cortical neurons expressing the EB3-GFP fusion protein. The movie is composed of 300 stills taken every 2 seconds over a period of 10 minutes. Moving EB3-GFP comets are less numerous in $Sp^{\Delta/\Delta}$ axons compared to control axons.

Movie 4: Live imaging of dynamic microtubule plus ends in a DIV6 $Sp^{\Delta/\Delta}$ axonal swelling. The boxed region indicates the axonal swelling used for kymograph analysis in the middle panel of Fig. 5E.

Movie 5: Live imaging of dynamic microtubule plus ends in a DIV6 $Sp^{\Delta/\Delta}$ axonal swelling. The boxed region indicates the axonal swelling used for kymograph analysis in the right panel of Fig. 5E.

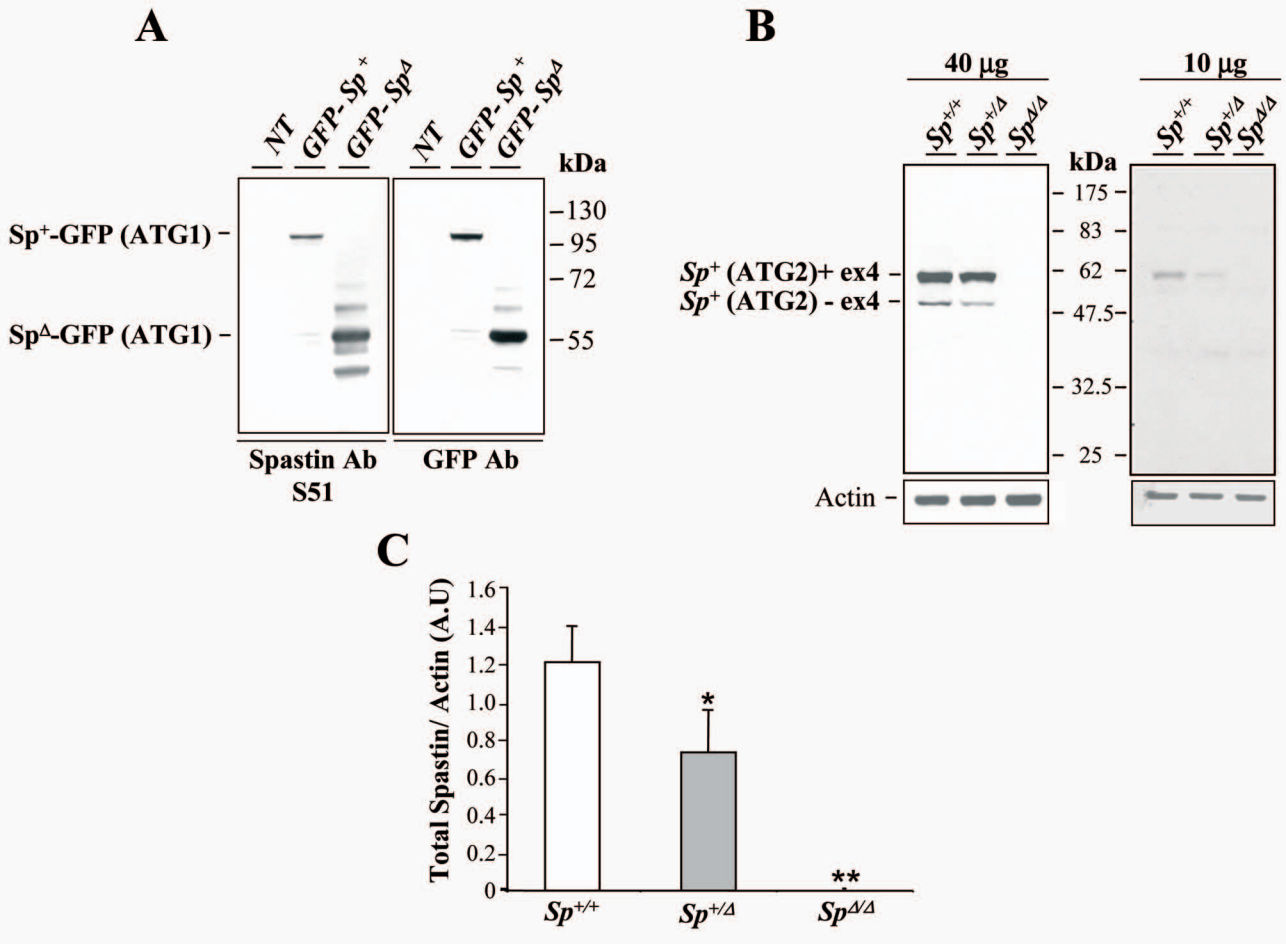
A
NT
GFP-Sp+
GFP-SpΔ
NT
GFP-Sp+
GFP-SpΔ
kDa
130
95
72
55
Sp+-GFP (ATG1)
SpΔ-GFP (ATG1)
Spastin Ab
S51
GFP Ab
B
40 µg
10 µg
Sp+/+
Sp+/Δ
SpΔ/Δ
Sp+/+
Sp+/Δ
SpΔ/Δ
kDa
175
83
62
47.5
32.5
25
Sp+ (ATG2)+ ex4
Sp+ (ATG2) - ex4
Actin
C
Total Spastin/ Actin (A.U)
1.6
1.4
1.2
1.0
0.8
0.6
0.4
0.2
0
*
**
Sp+/+
Sp+/Δ
SpΔ/Δ

Figure 1

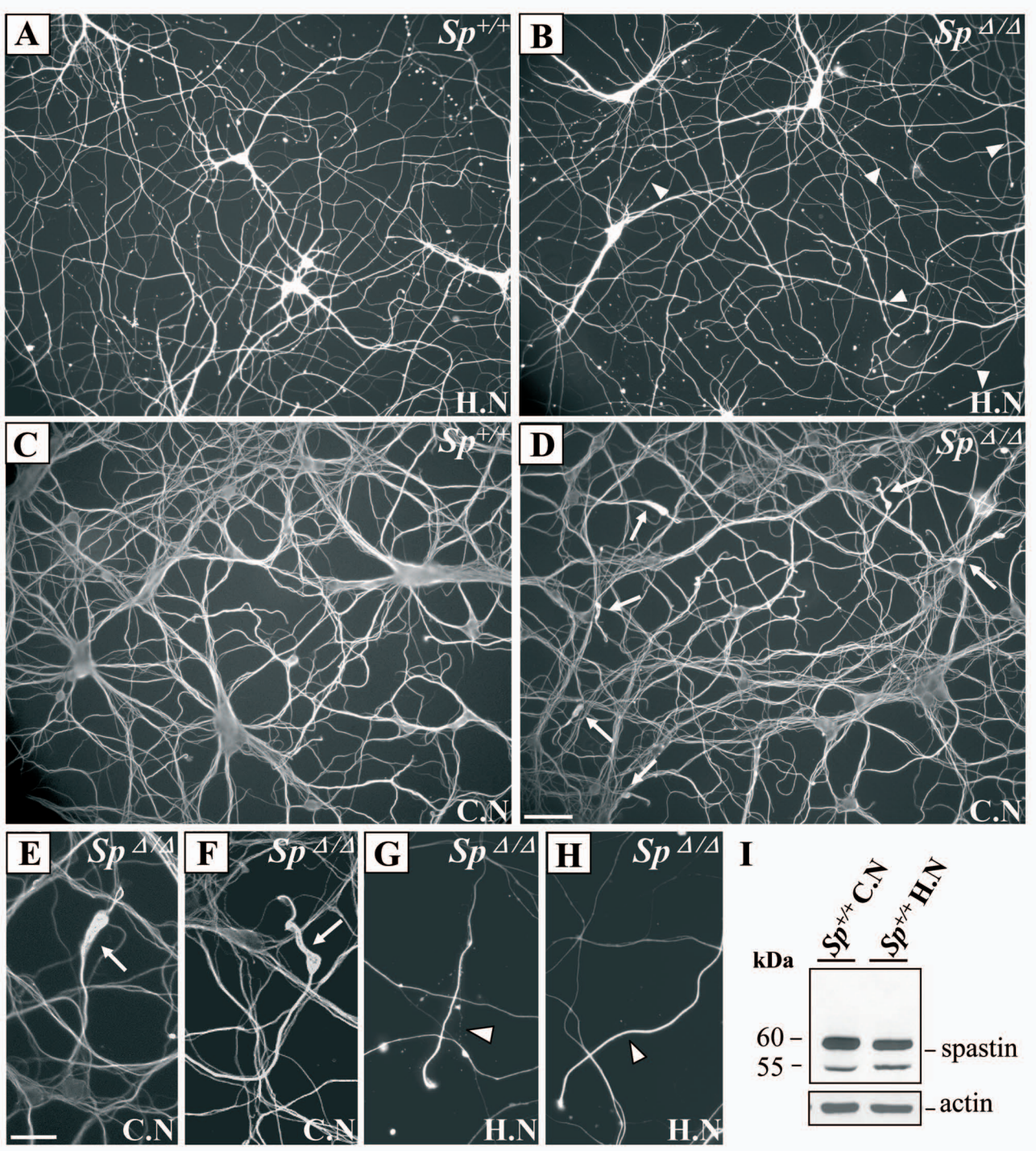
A
Sp+/+
H.N
B
Sp Δ/Δ
H.N
C
Sp+/+
C.N
D
Sp Δ/Δ
C.N
E
Sp Δ/Δ
C.N
F
Sp Δ/Δ
C.N
G
Sp Δ/Δ
H.N
H
Sp Δ/Δ
H.N
I
Sp+/+ C.N
Sp+/+ H.N
kDa
60
55
spastin
actin

Figure 2

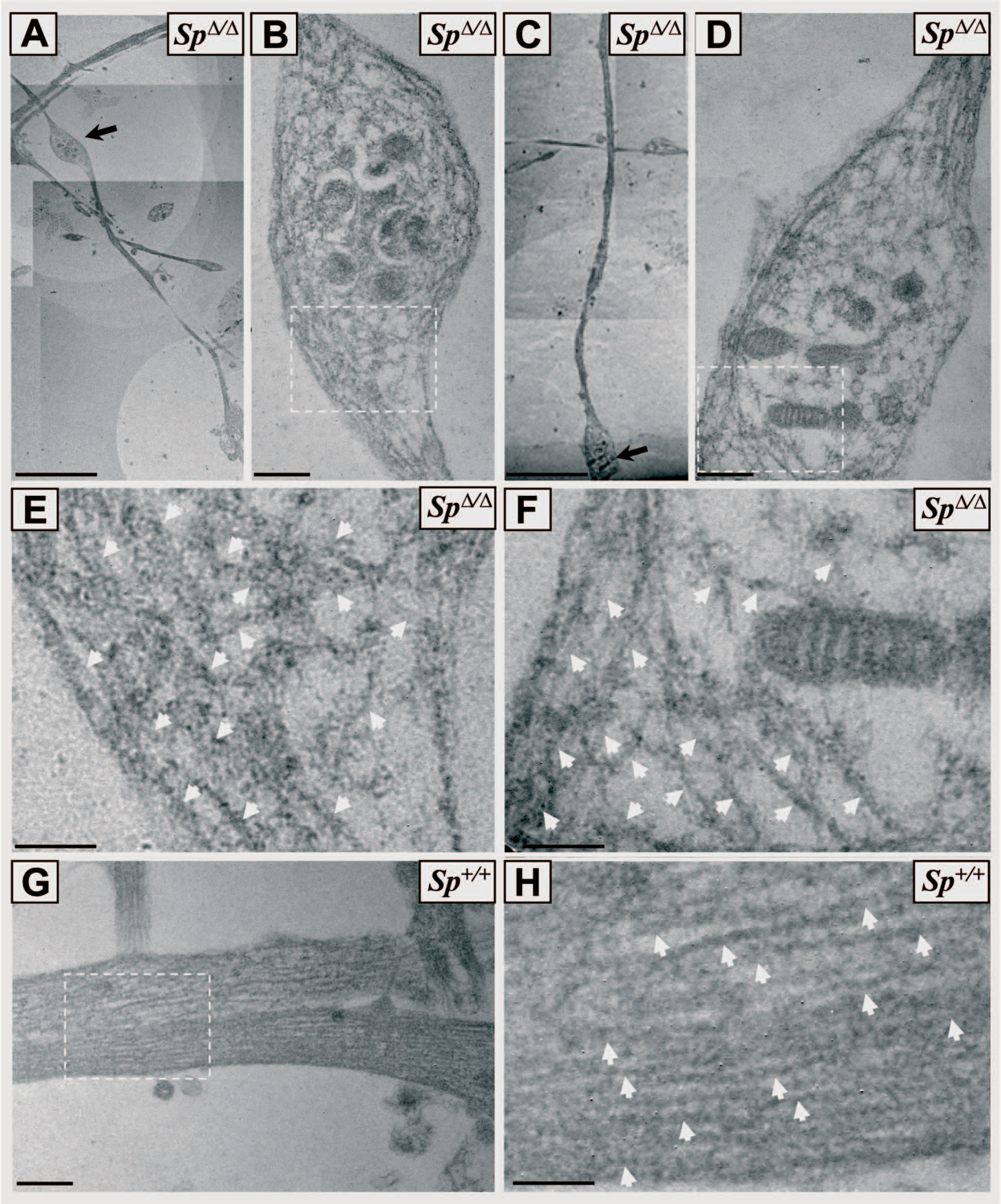

Figure 3

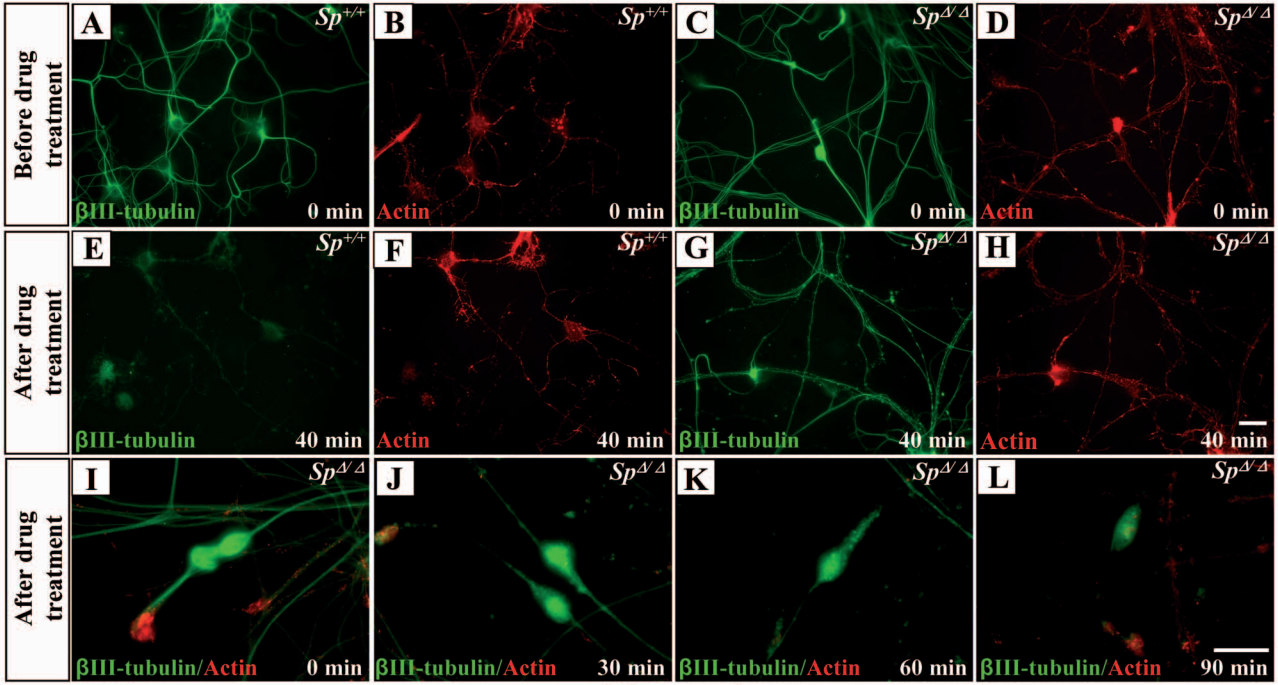
Before drug treatment
After drug treatment
After drug treatment
A
Sp+/+
βIII-tubulin
0 min
B
Sp+/+
Actin
0 min
C
SpΔ/Δ
βIII-tubulin
0 min
D
SpΔ/Δ
Actin
0 min
E
Sp+/+
βIII-tubulin
40 min
F
Sp+/+
Actin
40 min
G
SpΔ/Δ
βIII-tubulin
40 min
H
SpΔ/Δ
Actin
40 min
I
SpΔ/Δ
βIII-tubulin/Actin
0 min
J
SpΔ/Δ
βIII-tubulin/Actin
30 min
K
SpΔ/Δ
βIII-tubulin/Actin
60 min
L
SpΔ/Δ
βIII-tubulin/Actin
90 min

Figure 4

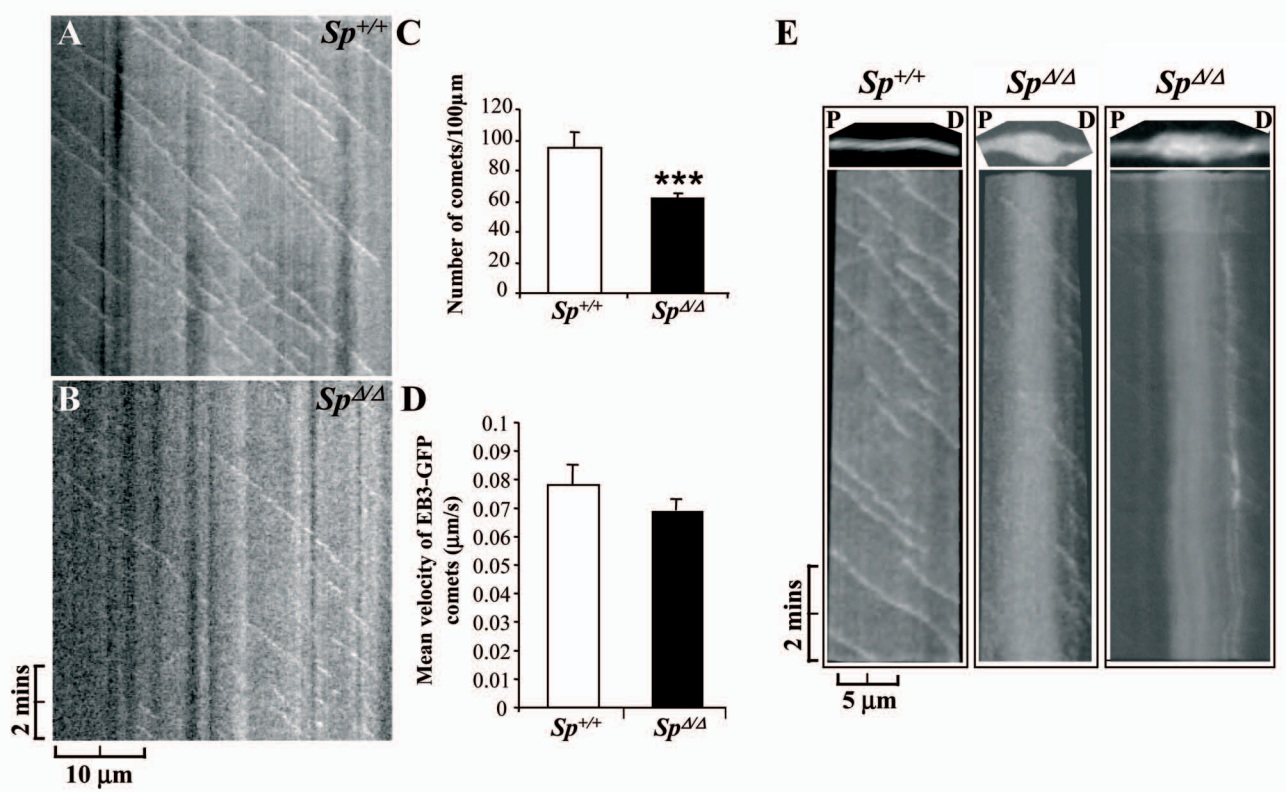
A
Sp+/+
B
SpΔ/Δ
2 mins
10 µm
C
Number of comets/100µm
120
100
80
60
40
20
0
***
Sp+/+
SpΔ/Δ
D
Mean velocity of EB3-GFP comets (µm/s)
0.1
0.09
0.08
0.07
0.06
0.05
0.04
0.03
0.02
0.01
0
Sp+/+
SpΔ/Δ
E
Sp+/+
SpΔ/Δ
SpΔ/Δ
P
D
2 mins
5 µm

Figure 5

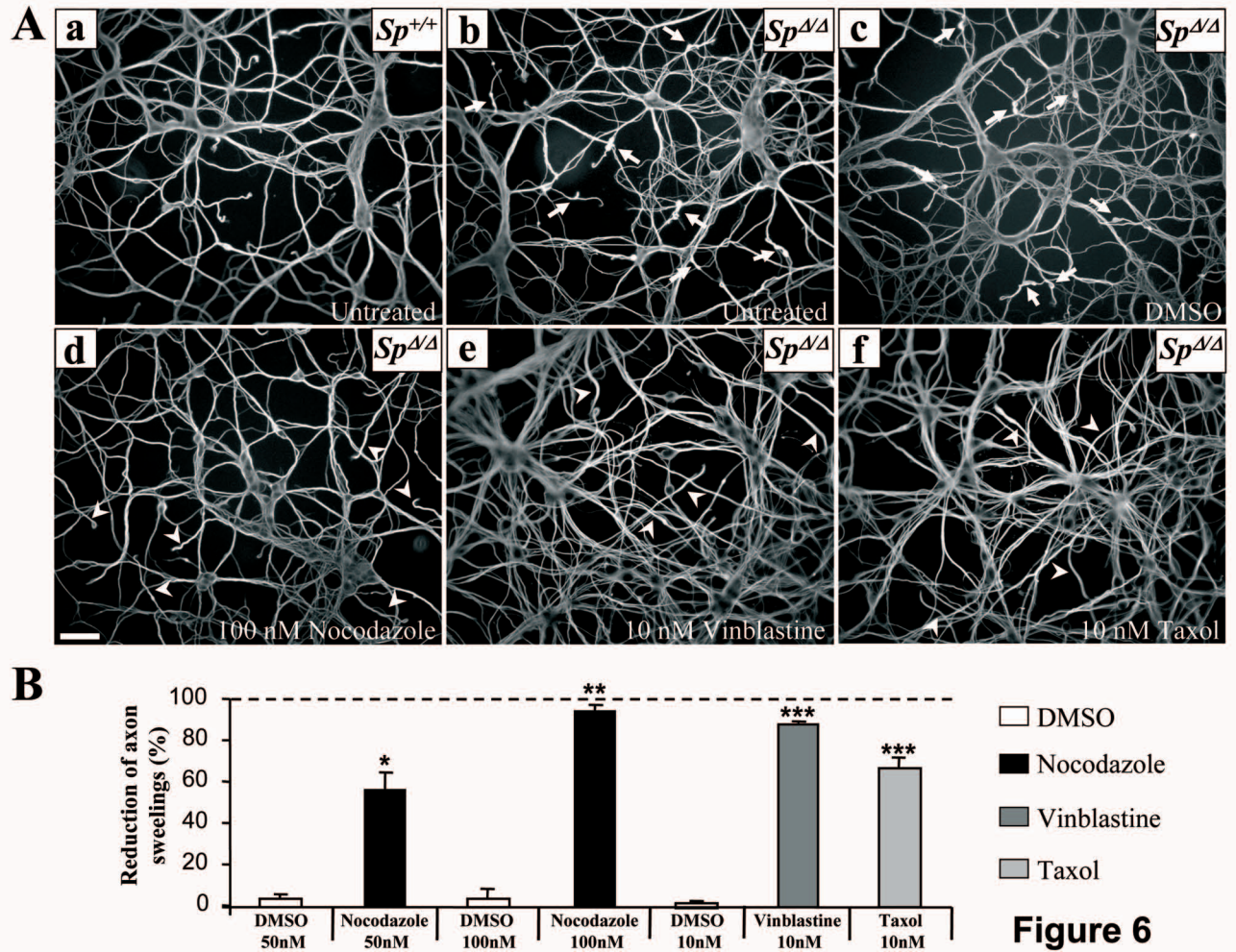
A
a
Sp+/+
Untreated
b
SpΔ/Δ
Untreated
c
SpΔ/Δ
DMSO
d
SpΔ/Δ
100 nM Nocodazole
e
SpΔ/Δ
10 nM Vinblastine
f
SpΔ/Δ
10 nM Taxol
B
Reduction of axon sweelings (%)
100
80
60
40
20
0
*
**
***
***
DMSO 50nM
Nocodazole 50nM
DMSO 100nM
Nocodazole 100nM
DMSO 10nM
Vinblastine 10nM
Taxol 10nM
DMSO
Nocodazole
Vinblastine
Taxol

Figure 6

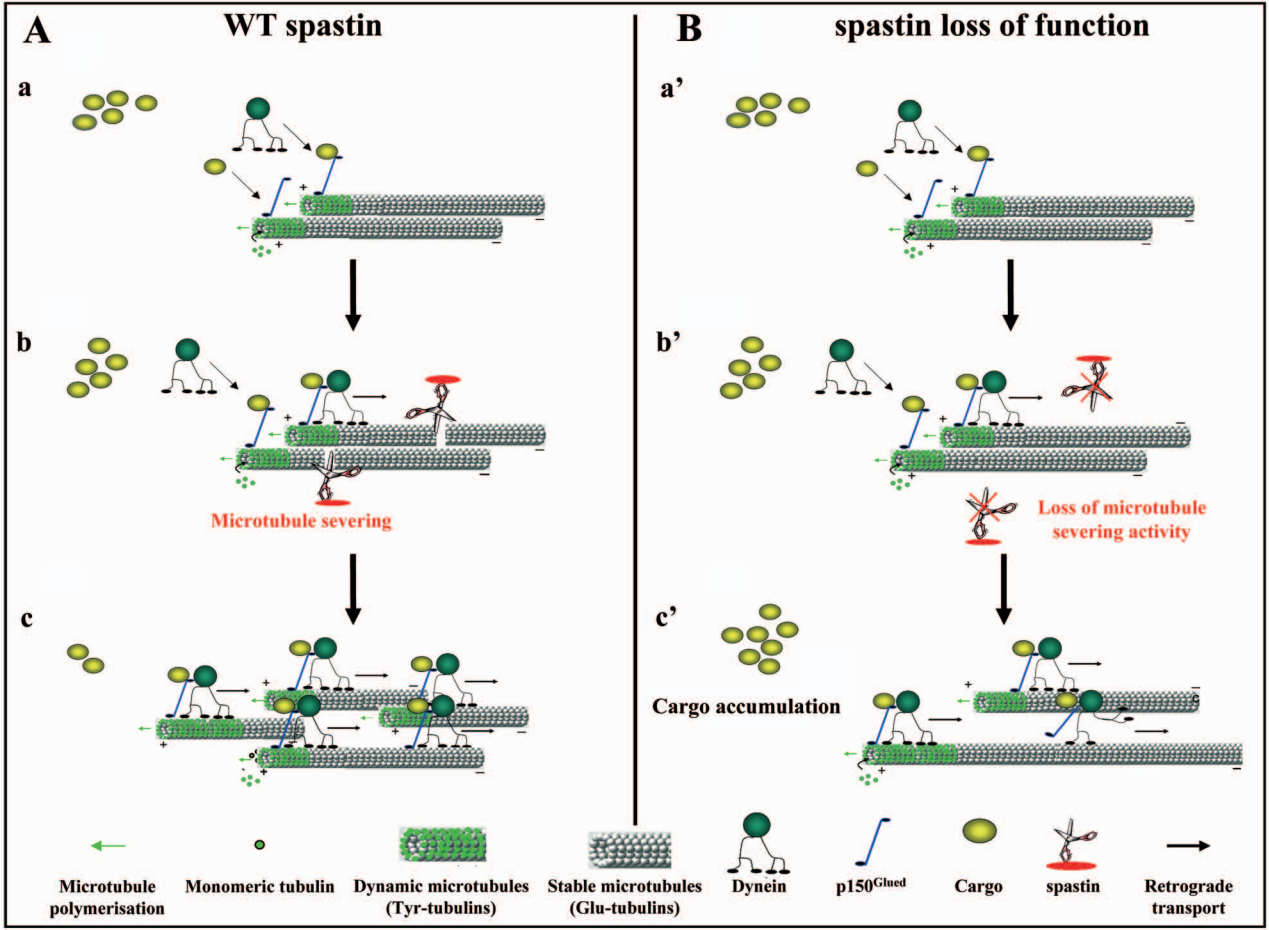
A
WT spastin
B
spastin loss of function
a
b
c
a'
b'
c'
Microtubule severing
Loss of microtubule severing activity
Cargo accumulation
Microtubule polymerisation
Monomeric tubulin
Dynamic microtubules (Tyr-tubulins)
Stable microtubules (Glu-tubulins)
Dynein
p150Glued
Cargo
spastin
Retrograde transport

Figure 7

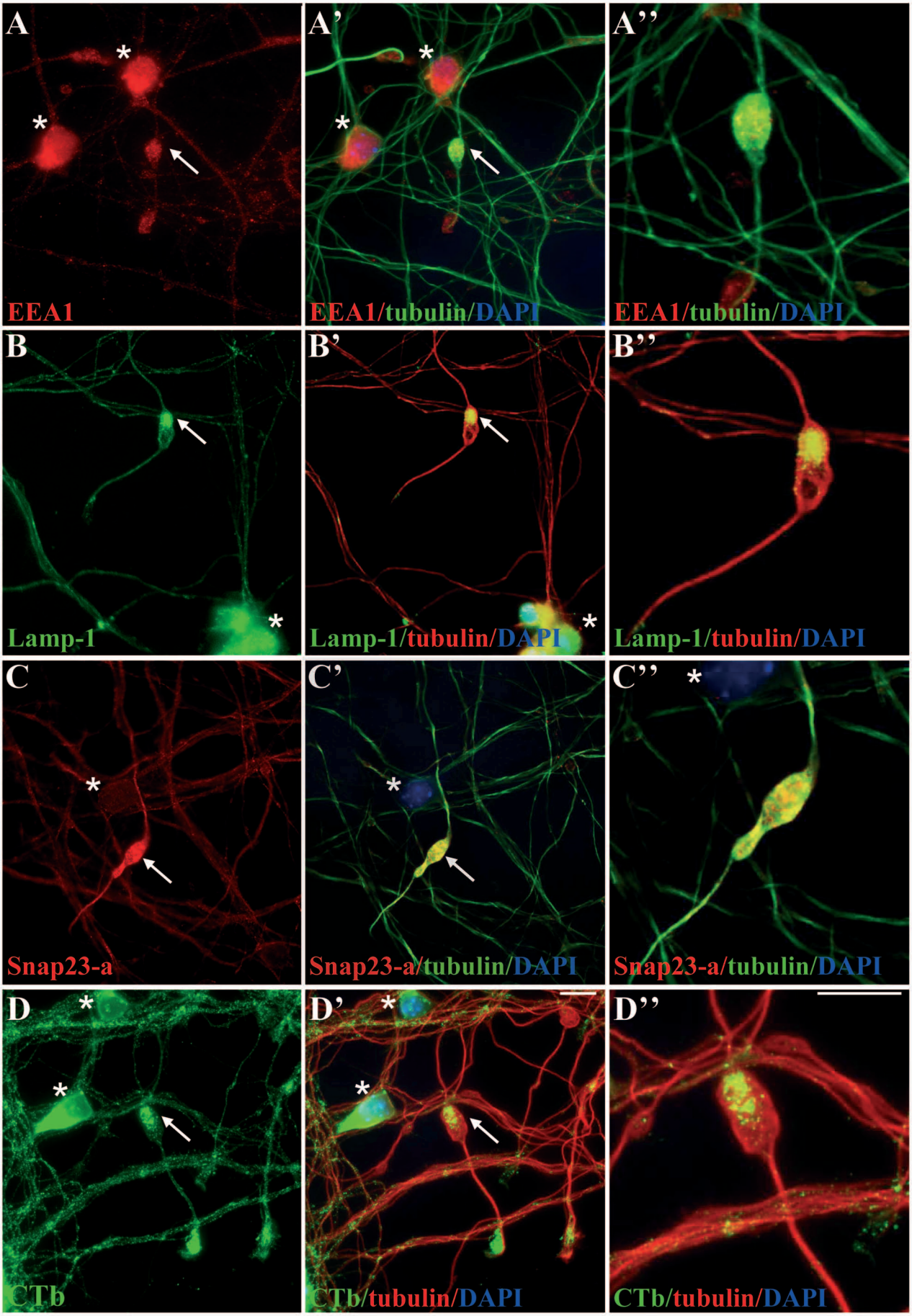
A
EEA1
A'
EEA1/tubulin/DAPI
A''
EEA1/tubulin/DAPI
B
Lamp-1
B'
Lamp-1/tubulin/DAPI
B''
Lamp-1/tubulin/DAPI
C
Snap23-a
C'
Snap23-a/tubulin/DAPI
C''
Snap23-a/tubulin/DAPI
D
CTb
D'
CTb/tubulin/DAPI
D''
CTb/tubulin/DAPI

Figure S1

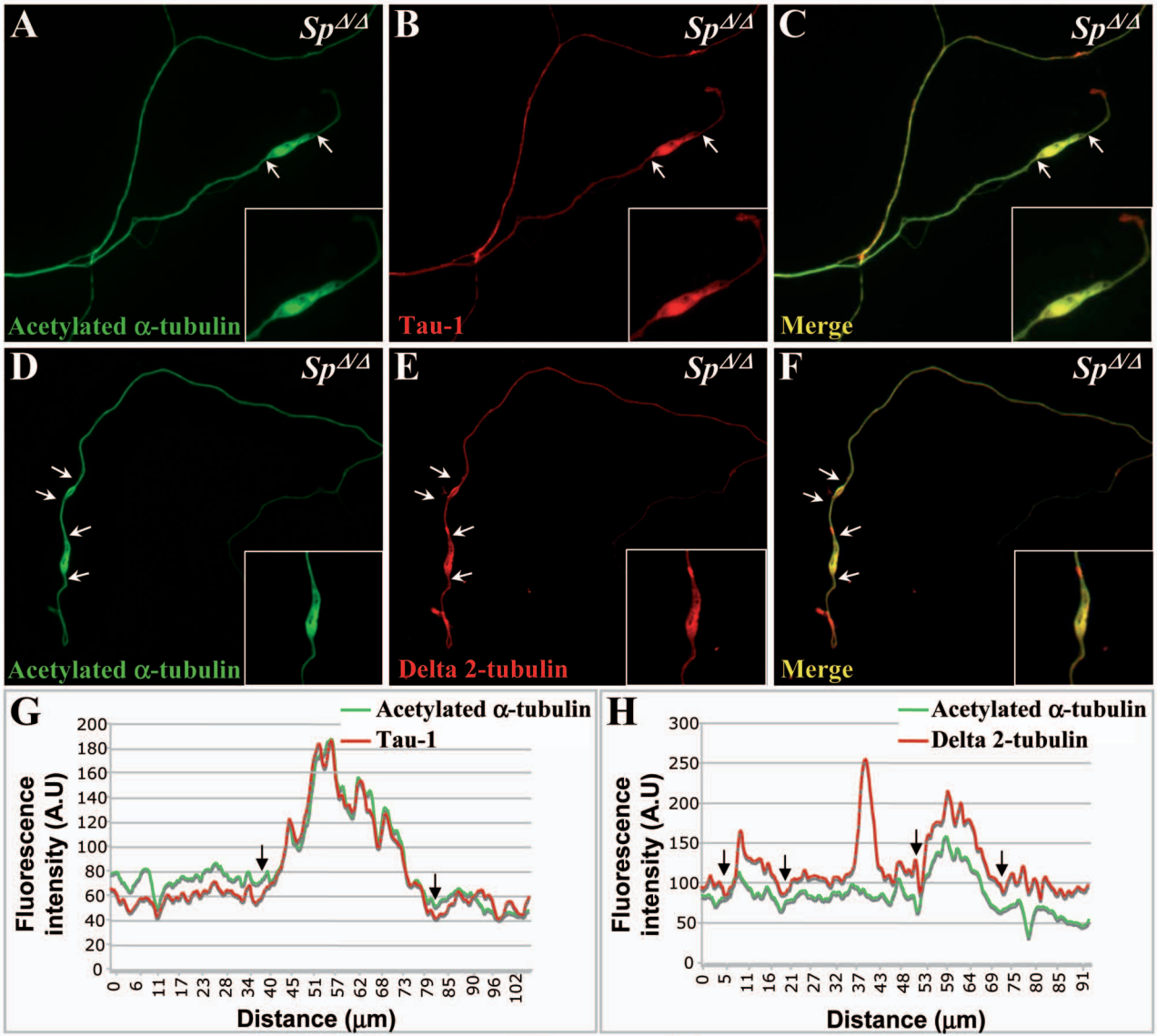
A
Sp^Δ/Δ
Acetylated α-tubulin
B
Sp^Δ/Δ
Tau-1
C
Sp^Δ/Δ
Merge
D
Sp^Δ/Δ
Acetylated α-tubulin
E
Sp^Δ/Δ
Delta 2-tubulin
F
Sp^Δ/Δ
Merge
G
Acetylated α-tubulin
Tau-1
Fluorescence intensity (A.U)
Distance (μm)
H
Acetylated α-tubulin
Delta 2-tubulin
Fluorescence intensity (A.U)
Distance (μm)

Figure S2

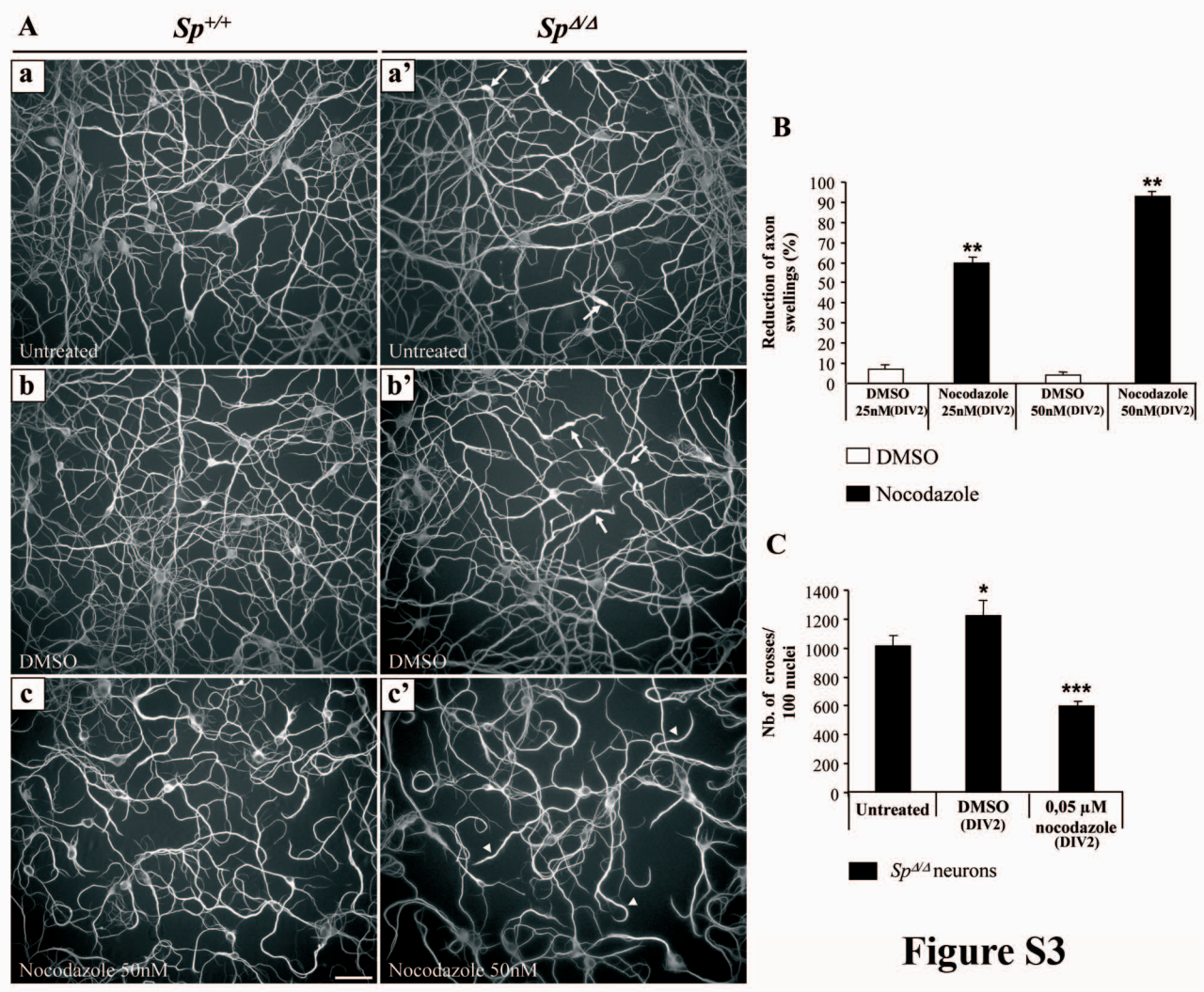
A
Sp+/+
SpΔ/Δ
a
a'
Untreated
Untreated
b
b'
DMSO
DMSO
c
c'
Nocodazole 50nM
Nocodazole 50nM
B
Reduction of axon swellings (%)
100
90
80
70
60
50
40
30
20
10
0
**
**
DMSO 25nM(DIV2)
Nocodazole 25nM(DIV2)
DMSO 50nM(DIV2)
Nocodazole 50nM(DIV2)
DMSO
Nocodazole
C
Nb. of crosses/ 100 nuclei
1400
1200
1000
800
600
400
200
0
*
***
Untreated
DMSO (DIV2)
0,05 µM nocodazole (DIV2)
SpΔ/Δ neurons

Figure S3